UNIVERSITY OF OKLAHOMA

GRADUATE COLLEGE

ENHANCEMENT OF ZEOLITE CATALYZED REACTIONS

FROM WATER CLUSTERS AND BRONSTED SITE PROXIMITY

A THESIS

SUBMITTED TO THE GRADUATE FACULTY

in partial fulfillment of the requirements for the

Degree of

MASTER OF SCIENCE

By

MICHAEL ZEETS
Norman, Oklahoma
2018

ENHANCEMENT OF ZEOLITE CATALYZED REACTIONS
FROM WATER AND BRONSTED SITE PROXIMITY

A THESIS APPROVED FOR THE
SCHOOL OF CHEMICAL, BIOLOGICAL AND MATERIALS ENGINEERING

BY

_____
Dr. Bin Wang, Chair

_____
Dr. Daniel Resasco

_____
Dr. Steven Crossley

To my parents, family, and loving girlfriend, who supported me in my education and research every step of the way, even when they had some confusion on what exactly my project was about.

Acknowledgements

Table of Contents

List of Tables

List of Figures

Abstract

Zeolites offer many benefits as a catalyst. The adjustable acid sites in zeolites and its well-defined pore structure allows for a fine-tuning of the catalytic performance. The activity and selectivity of several reactions have been shown to be dependent on the location and distribution of the acid sites in the zeolite. However, the underlying mechanisms responsible for this dependence remain to be explored. In this thesis, using density functional theory (DFT) calculations, the impact of proximity of Brønsted acid sites in zeolite HZSM-5 as well as the role of water in enhancing catalytic reactions is investigated.

It is found that Brønsted sites with close spatial proximity can significantly strengthen the adsorption of water, which is used as a molecular probe for the local activity. It is shown that a water molecule can form H-bonds with two adjacent sites with increased adsorption energy. Following on this, ab initiomolecular dynamics simulations are used to analyze water interactions with acid sites, and the charge stabilizing effect of water clusters are shown. This charge stabilization as well as the polarization effect of nearby acid sites are proposed as the causes behind a series of water enhanced reactions at zeolites with high acid site densites.

The catalytically beneficial effects of water cluster interaction and acid site polarization of n-hexane cracking in HZSM-5 was studied using DFT Nudged Elastic Band (NEB) kinetic barrier calculations. Water showed potential for reaction enhancement, appearing to stabilize the charged intermediate by forming hydrogen bonds with the reverse zeolite wall. Nearby acid sites also showed enhancement. One would polarize the hexane while the other participated in the protonation. With the two

beneficial effects in combination the benefits compounded, with a greater result than the sum of their parts. The results are far from conclusive but they are very promising if consistent enhancement can be achieved.

Chapter 1: Introduction

1.1 Zeolites & ZSM-5

Zeolites are one of the most widely used catalysts in industry. Because of the well-defined small pore sizes and tunable acid sties, zeolites have been applied in separation and catalysis processes such as oil refining, petrochemistry, and organic synthesis. The focus of this project is on ZSM-5, a zeolite with particularly widespread use in conversion of hydrocarbons in the petrochemical industry. The entirety of the zeolite structure is a crystalline aluminosilicate, composed of TO_4 tetrahedra (T = Si, Al) with the O atoms connecting neighboring tetrahedra. 10-member silicon rings form micropores throughout the structure. These small pore sizes make it very useful as a molecular sieve and catalyst, only allowing relatively small molecules to pass and giving high size-specific selectivity.[1]
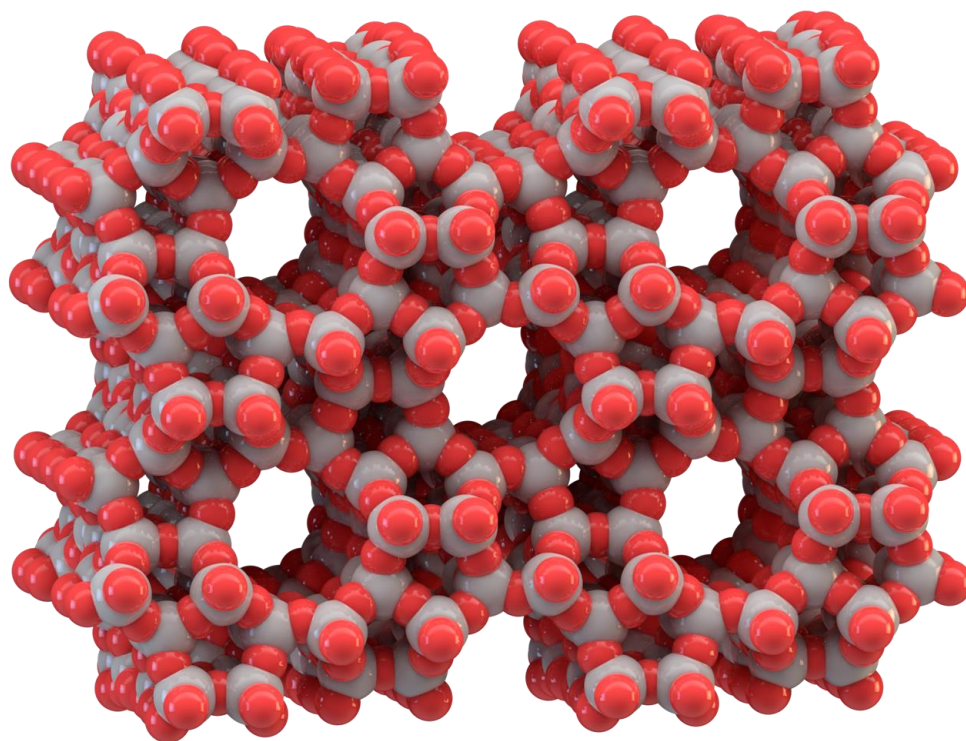
Figure 1: The Microporous Molecular Structure of a Zeolite, ZSM-5. This figure was taken from an article by Dr. Splettstoesser.[2]

Zeolites are a type of acid catalyst but not in the silicate form shown by Figure 1. The acidic form is titled HZSM-5 and has highly active Brønsted acid sites (BAS), in which the silica framework contains substituted aluminum atoms. These are normally counterbalanced by protons bonding to one of the neighboring oxygen forming the BAS. Upon incorporation of Al into the silica framework, the +3 charge on the Al makes the framework negatively charged, and requires the presence of extraframework cations, such as H^+, within the structure to keep the overall framework neutral. A graphic of this can be seen below in Figure 2. The extraframework cations are ion exchangeable and give rise to the rich ion-exchange chemistry of these materials, with the novelty of zeolites stemming from their microporosity and the unique topology of the framework.[1] The intrinsic properties of these active sites, such as the acid strength and molecular confinement within the micropores are of great interest in catalyst design.[3]
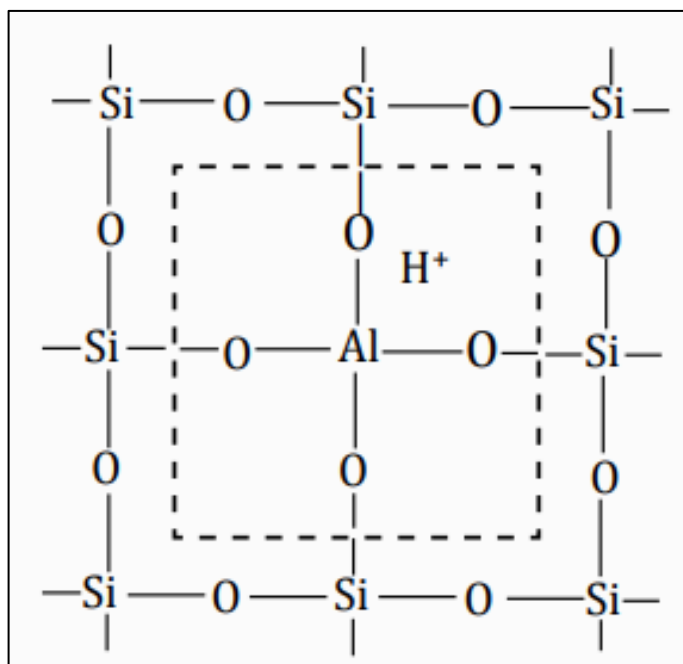
Figure 2: Form of Zeolite Brønsted Acid Sites. This figure was taken from a textbook by Drs. Hattori and Ono.[4]

The unit cell of ZSM-5 has 96 tetrahedral sites (T sites) of silicon and 192 oxygen atoms. The pore network is composed of two types of interconnected perpendicular channels, one of them straight and the other sinusoidal, weaving perpendicularly to each other. Of the 96 T sites, there are 12 symmetrically distinguishable T site locations that can be occupied by Al. Ghorbanpour et al. looked at every site configuration possible using density functional theory (DFT) simulation and found that theoretical investigations of HZSM-5 require a careful selection of the active site.[5] Because some sites will be inherently less stable and less likely to be the actual site for reaction, having a realistic starting point is important to ensure the relevance of the calculation. Even then, where the acid sites are actually located in reality is highly dependent on zeolite synthesis techniques, reaction conditions, and any number of other complications.

Density of these acid sites have been shown to play significant roles in zeolite catalysis.[6] When discussing acid site density, a common phrase is the Si/Al ratio. Since the BAS are where the aluminum substitutes, the Si/Al ratio is a quick and easy way to quantify acid site density. A lower Si/Al ratio means more Al have substituted and thus a higher acid site density. This doesn't necessarily correlate to local density on a molecular scale but in general acid sites as charged locations should spread out throughout the zeolite structure at a similar composition as the Si/Al ratio. Intriguingly, previous studies have shown modified catalytic selectivities and improved catalyst activity beyond the expected proportional improvement of the reaction rate to number of sites, implying the important role of site location and distribution.[7-10] Deeper understanding of the structure of ZSM-5 and the impact of BAS placement at distinct locations is important to fully understand what is taking place during reaction.

Distribution of these acid sites must also be considered. The internal volume of zeolites consists of interconnected cages or channels. The framework can exhibit some flexibility with changes in temperature or via diffusing molecules. ZSM-5, also known by its framework type MFI consists of two types of intersecting 10-membered-ring pores. The geometry and size of these perpendicular pores differ: one type consists of straight channels with a size of 5.3×5.6 Å^2, the other has a tortuous shape, commonly referred to as the sinusoidal channels, with a size of 5.1×5.5 Å^2.[11] Such differences in pore size and local environment can trigger different adsorption properties between the two types of pores or even the intersection between them. Such a slight change in pore dynamics makes a large difference when it comes to reactions. Diffusion, confinement, accessibility, and activity are all likely to change based on the location of an acid site in the zeolite framework.

Zeolites in general have far too many unknowns and uncertainties in the structure, acid strength, and confinement for optimizing reactions conditions to be an easy task. However, the importance and strong purpose of zeolites in the petrochemical and other industries makes this challenge well worth undertaking. For decades this catalyst and details of reactions involving it have been the focus of many research groups and companies across the world. In that regard this project is only a drop in the bucket. The rest of the introduction will go over the basics of the theory behind calculations and provide an idea of what motivated this project and what will be the focus amongst all the potential questions that could be asked about zeolite catalysis.

1.2 Density Functional Theory (DFT)

This project is completely composed of calculations done using the Vienna Ab initio Simulation Package (VASP) to compute the ground state properties using density functional theory (DFT). This project doesn't delve too deeply into the details of these calculations but regardless it is important to discuss what exactly is being solved. Specific computational methods will be detailed in each section separately, with subsections in the introductions describing specific calculations done for the following results.

DFT is one of the most popular and successful quantum mechanical approaches to matter. It is nowadays routinely applied for calculating the binding energy of molecules in chemistry and the band structure of solids in physics.[12] In its most basic form it is simply solving Schrödinger's Equation. All information about a given system is contained in the system's wave function, Ψ. The nuclear degrees of freedom (e.g., the crystal lattice in a solid) appear only in the form of a potential v(r) acting on the electrons, so that the wave function depends only on the electronic coordinates.[12] This wave function is calculated from Schrödinger's equation, which for a single electron moving in a potential v(r) is

$$\left[-\frac{\hbar^2 \nabla^2}{2m} + \boldsymbol{v(r)} \right] \boldsymbol{\psi(r)} = \boldsymbol{\epsilon * \psi(r)}$$

If there is more than one electron (i.e., one has a many-body problem) Schrödinger's equation becomes

$$\left[\sum_i^N \left(-\frac{\hbar^2 \nabla_i^2}{2m} + \boldsymbol{v(r_i)} \right) + \sum_{i<j} U(r_i, r_j) \right] \boldsymbol{\psi(r_1, r_2, \dots, r_N)} = \boldsymbol{E\psi(r_1, r_2 \dots, r_N)}$$

where N is the number of electrons and $U(r_i, r_j)$ is the electron-electron interaction.

For a system of particles interacting via Coulomb interaction, this electron-electron interaction looks like

$$\hat{U} = \sum_{i<j} U(r_i, r_j) = \sum_{i<j} \frac{q^2}{|r_i - r_j|}$$

Whether the system is an atom, a molecule, or a solid it only depends only on the potential $v(r_i)$.[12] The specifics get more complex than this but at its root DFT is fairly straightforward. It is the many-body system with hundreds or thousands of electrons where the calculation becomes extremely complex and computationally expensive.

The usual quantum-mechanical approach to Schrödinger's equation can be summarized by the following sequence as given by Capelle et al.

$$v(\mathbf{r}) \xrightarrow{SE} \Psi(\mathbf{r}_1, \mathbf{r}_2 \ldots, \mathbf{r}_N) \xrightarrow{\langle \Psi | \ldots | \Psi \rangle} \text{observables,}$$

Basically, one specifies the system by choosing $v(r)$, plugs it into Schrödinger's equation, solves that equation for the wave function Ψ, and then calculates "observables" by taking expectation values of operators with this wave function.[12] Many powerful methods for solving Schrödinger's equation have been developed during decades of struggling with the many-body problem. The problem with these methods is the great demand they place on one's computational resources: it is simply impossible to apply them efficiently to large and complex systems.

It is here where DFT provides a viable alternative, which is also much more versatile. One of the "observables" found by the standard quantum mechanical approach is the particle density $n(r)$. DFT simplifies the calculation by promoting $n(r)$ from an "observable" to a key variable. From this one can approach the problem in what is basically the reverse order as the standard quantum-mechanical approach.

6

This approach forms the basis for most of electronic-structure calculations in physics and chemistry.[12] The specifics of that approach vary based on the type of application, but the base idea of the equation for getting wavefunction from n(r) is as follows

$$n(\vec{r}) = N \int d^3 r_2 \cdots \int d^3 r_N \psi^*(\vec{r}, \vec{r}_2, \ldots, \vec{r}_N) * \psi(\vec{r}, \vec{r}_2, \ldots, \vec{r}_N)$$

and the density-functional approach can be summarized by the sequence

$$n(\mathbf{r}) \implies \Psi(\mathbf{r}_1, \ldots, \mathbf{r}_N) \implies v(\mathbf{r}),$$

Knowledge of n(r) implies knowledge of the wave function and the potential, and hence of all other observables.[12] Although this sequence describes the conceptual structure of DFT, it does not really represent what is done in actual applications of it, which typically proceed along rather different lines, and do not make explicit use of many-body wave functions. From this groundwork, changes can be made to fit the problem at hand and give DFT a very wide degree of usefulness for those in any science discipline but particularly physics or chemistry atomic based calculations such as those done in this text.

For nearly every calculation presented in this text, DFT will be used to "optimize" the energy of a certain combination and configuration of molecules by finding the lowest combined energy state. Using either this energy or the resulting structure that DFT deems the most energetically stable conclusions will be drawn on how molecules are most likely to interact with each other and how this can be manipulated or improved. From these calculations, one can gain insight into any number of different trends relevant to real world systems.

1.3 Project Motivation and Scope

Factors that enhance zeolite-catalyzed reactions and the reasons for them doing so haven't been fully explored. As discussed previously, the immense impact of these catalysts on petrochemical reactions means that any enhancement however small is worth pursuing to better understand their mechanisms.

Promising results such as Chen et al. show that controlled addition of sub-stoichiometric amounts of water led to nearly an order of magnitude increase in benzene reaction rate.[13] Interestingly, this enhancement only took place at high aluminum density (Si/Al ratio of 15) and the enhancement quickly dropped off with higher water loading. The decrease at higher loading can be easily explained as the competitive adsorption of water inhibiting the benzene reaction, but the curiosity is that there was an enhancement at all and why it was only seen at high acid density. The study suggests that the water enhancement effect is due to a "vehicle hopping" proton transfer effect, which cannot occur when acid sites are isolated.[13]

An intriguing result was found by OU alum Dr. Abhishek Gumidyala.[14] While testing n-hexane cracking over HZSM-5, with the addition of water a huge leap in conversion was achieved. Once again, this enhancement only took place at high aluminum density and it quickly dropped off with higher water loading. At its peak, however, there was nearly a doubling of the conversion possible at those reaction conditions. Figures showing this enhancement can be seen on the next page as Figure 3 and 4.
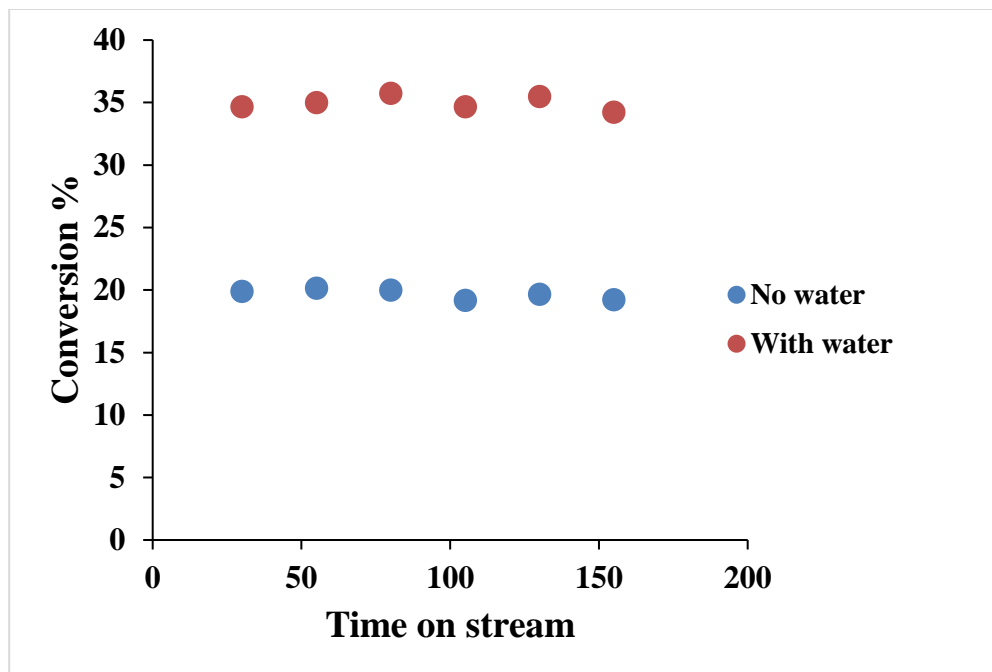
Figure 3: N-hexane cracking conversion as a function of time, both with and without water. This and the following plot was provided by Dr. Gumidyala.[14]
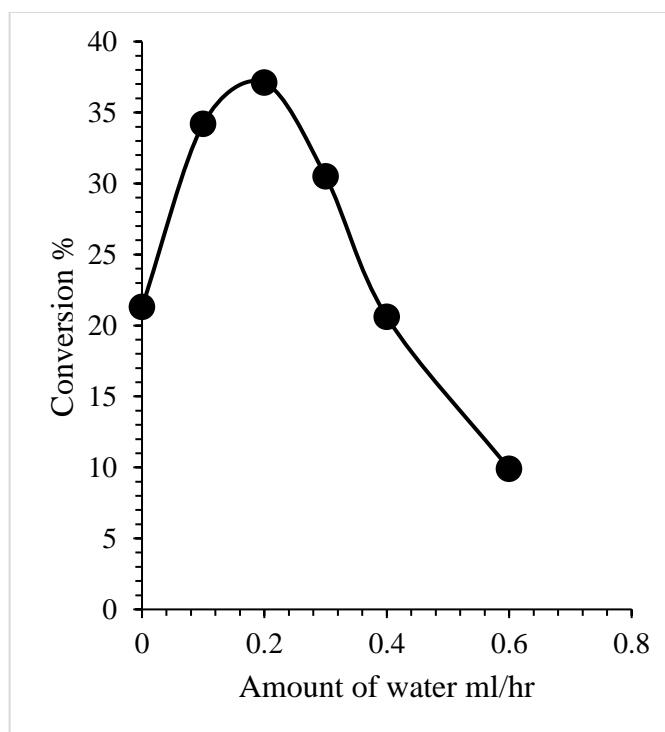
Figure 4: N-hexane cracking conversion on HZSM-5 as a function of amount of water. The highest point on this figure is the data used for Figure 3.[14]

The primary goal of this project is to use DFT simulation to investigate the water enhancement phenomena on zeolites such as those found by Dr. Gumidyala[14] and Chen et al.[13] and provide a greater understanding of what might be taking place. The specific focus of this research was the impact of BAS proximity to each other as a possible explanation of why the results were only seen at low Si/Al. A few different approaches were taken to tackle the beneficial effect of water. The results will be discussed in the following chapters, but details of it will be listed here to explain the train of thought that led to the decisions that were made.

The work began and shown in Chapter 2 is as follows. Ghorbanpour et al.[5] was used as a basis in order to identify all of the T sites of HZSM-5 and then expanded upon to check the effect of site configuration. Based on the recommendation of this article, site T7 was used as the starting point for calculations since it is the most stable. Next, insight on how proximity between two BAS sites affects molecular adsorption was gained through calculations using water as a probe molecule. By varying the distance between sites, the difference in chemical activity of isolated and clustered BAS in HZSM-5 was found. This compared favorably to experimental adsorption energy results as found by Ohlin et al.[15]. The adsorption of the nonpolar molecule hexane was also calculated on an adjacent and isolated BAS to see if the same benefits carried over. The water molecule is polarized, as evidenced by significant charge redistribution. This is similar to the predicted polarization on acetone and alkanes as done by Song et al.[16]. Interestingly, it was found that the proton of one of the two BAS may become delocalized and a hydronium ion is formed when interacting with adjacent acid sites, similar to that of the water cluster found by Vjunov et al.[17].

Both the enhanced polarization and proton delocalization were determined as possible causes for activity and selectivity enhancement in zeolite-catalyzed reactions. The importance of using hybrid functional calculations when comparing stability of configurations with two acid sites separated by varied distance was examined. They did not change the results but was important to be sure the calculations were not flawed.

The Chapter 3 is focused on water clusters as detailed by Vjunov et al.[17], the difference is that these calculations will be ab initio molecular dynamics (AIMD) simulations at 320K using close proximity Bronsted sites to see if one or both protons go into the cluster and how the charge is delocalized amongst the water molecules. There is also a tangential AIMD simulation looking at if water preferentially occupies the sinusoidal channel. This has been claimed in experimental studies such as that done by Kubarev et al.[11] and is not influential to the primary goal of the project but it provides some insight into how water occupies the zeolite during regular conditions.

In Chapter 4 the focus is on a zeolite catalysis reaction itself. The reaction focused on this project was protolytic hexane cracking as such done by Dr. Gumidyala and using a specific mechanism as given by Boronat et al.[18]. By applying the two main theories generated of what is occurring, water clusters forming around sites stabilizing charged intermediates and nearby acid sites working to polarize and enhance adsorption, there was shown to be significant enhancement in the kinetics of the reaction. The extent of this kinetic analysis was limited to the barriers of the reaction, but this could be further expanded upon in the future.

Chapter 2: Enhancement of Chemical Adsorption for Adjacent Acid Sites

2.1 Introduction

As mentioned in Chapter 1, density and distribution of the acid sites play significant roles in zeolite catalysis.[6, 19] While the density of the acid sites is determined by the framework Si/Al ratio, the distribution of these acid sites is controlled by nucleation and growth kinetics during the hydrothermal synthesis[9], which in turn determine whether they are placed as either isolated or paired sites in the framework. Therefore, the pairing of sites can be manipulated to some extent by changing the structure-directing agents during the synthesis[19-23] and upon post-treatment methods such as zeolite steaming[24]. Intriguingly, previous studies have shown modified catalytic selectivities and improved catalyst activity beyond the expected proportional improvement of the reaction rate to number of sites, implying the important role of site location and distribution.[7-10] The exact reasons for this extra activity improvement remain unclear.[25-30] Early quantum mechanical calculations using a cluster model suggest increased proton affinity, corresponding to reduced acidity, when two BAS are located in the proximity.[31, 32] This reported reduced acidity is in line with experimental work using NH$_3$-TPD to determine the ZSM-5 acidity.[7] However, using dehydration rate of CH$_3$OH as a probe, it has been shown that the rate constant is insensitive to the density of Al sites in MFI, suggesting that the acid strength of each isolated site remains the same within a certain range of acid site density.[28]

Alkane cracking is an important industrial process and has been shown in numerous studies that the distribution[16, 33-38] of BAS determines the activity and

selectivity. Cracking activity per site for hexane[39, 40] has been found to remain constant within a large range of Si/Al ratio in Zeolite Y and HZSM-5. Enhanced cracking rates have been reported when Si/Al is reduced, and may be attributed to non-homogeneous distribution of BAS into different confinement environment, which lead to modified apparent activation barrier and/or intrinsic activation barriers.[33, 36, 38, 41] More recently, Song et al. reported that adjacent BAS in HZSM-5 shows higher adsorption energies than isolated BAS for adsorption of acetones and alkanes due to enhanced polarization, which results in increased rate for alkane cracking in HZSM-5.[16] In addition, enhanced olefin oligomerization[10, 35] and hydrogen transfer[35] has also been attributed to BAS in the close proximity. It seems that adjacent BAS may have synergistic effect for molecular adsorption and reaction, though the underlying mechanism remains to be explored.

In this section, DFT calculations will be reported through which the chemical activity of isolated and clustered BAS in HZSM-5 is explored. By using a water molecule as a probe, the adsorption energy of a water molecule is shown to be significantly enhanced when two BAS are in close proximity, such as Al-O-$(Si-O)_1$-Al, and this enhanced water adsorption results from the increased H-bonding between water and the two BAS. The water molecule is polarized, as evidenced by significant charge redistribution. Interestingly, one of the two BAS is shown to become delocalized and a hydronium ion is formed when interacting with adjacent acid sites. Both the enhanced polarization and proton delocalization may affect activity and selectivity for zeolite-catalyzed reactions. The importance of using hybrid functional calculations when comparing stability of configurations with two acid sites separated by varied distance is also discussed.

2.1.1 Heat of Adsorption Calculations

The primary calculation done in this chapter is very simple, with the figure of analysis being the heat of adsorption. This calculation is simply the difference of the energies of the combined system and its separate components. The adsorption energy was calculated as $\Delta E_{ads} = E(water/HZSM-5) - E(water) - E(HZSM-5)$, where E(water/HZSM-5), E(water), E(HZSM-5) were the total energies of optimized configurations of water adsorption in HZSM-5, molecular water in vacuum, and HZSM-5 without water adsorption, respectively. This can be easily visualized as once the energy of the isolated water and zeolite are removed from the combined system, the difference remaining is the energy of the bond formed through adsorption.

2.1.2 Hybrid vs Explicit Functional

A concept discussed in this chapter is that of a hybrid functional. Hybrid functionals are a class of approximations to the standard functionals used in DFT. Essentially they are combining explicit functionals, in this case for hybrid functional HSE it is incorporating a portion of the explicit PBE functional with an error function screened Coulomb potential to calculate the exchange portion of the energy in order to improve computational efficiency and accuracy.[42]

This text will not delve into the specifics of why the hybrid HSE functional can be better suited for certain calculations but in general the standard PBE functional underestimates the repulsion felt by nearby charged sources such as the BAS in zeolites. This is known as a charge delocalization error. For this reason, it was necessary to check the results using hybrid calculations to be sure that they were reasonable.

2.2 Computational Methods

Calculations based on density functional theory (DFT) were carried out using the VASP (Vienna ab initio simulation) package.[43] The PBE generalized gradient approximation (GGA) exchange-correlation potential[44] was used, and the electron-core interactions were treated in the projector augmented wave method[45, 46]. The van der Waals interaction was taken into account through DFT-D3 semi-empirical methods via a pairwise force field.[47, 48] An HSE hybrid functional[49] was also used to calculate the total energy of structures that were already optimized by PBE-D3 calculations to reduce underestimation of the charge delocalization error of the semi-local PBE functional[50]. It has recently been shown that charge delocalization error in zeolite using the PBE functional caused quite significant changes in energy calculations as compared to values obtained using hybrid functionals.[51, 52] Note, as discussed later, all the compared adsorption enthalpy values are very similar between PBE and hybrid functional calculations, showing that the error was most likely cancelled out in the calculation of the adsorption enthalpy.

All the calculations were performed using a ZSM-5 unit cell including 96 Si and 192 O atoms. One Si atom at the T7 site, located at the intersection and more accessible to reactions[5], was the first replaced with an Al atom. The proton was initially attached to the O atom that was between the Al atom and T8 Si atom for reasons of minimizing energy as explained later by Table 2. The structure of the unit cell was taken from an experimental work (a = 20.078Å; b = 19.894Å; c = 13.372Å)[53] and fixed during the calculation. Atomic relaxation was performed using a single Γ point of the Brillouin zone

with a kinetic cutoff energy of 400 eV. All the atoms (zeolite and the molecules) were fully relaxed until the atomic forces were smaller than 0.02 eV Å^{-1}.

For the calculations of heat of adsorption, a water molecule was positioned at the aforementioned T7 site. When two sites were included in the calculations, the other T site was changed while the water was always positioned at the T7 site. In this way, the entropy contribution to the adsorption energy of water in zeolite doesn't change much since the relative position of the water molecule with respect to the zeolite framework remains the same. Therefore, though only calculated the adsorption enthalpy was calculated, we assume the Gibbs free energy follow the same trend assuming a similar entropy change. Changes to electron density were calculated based on the difference of the charge density between the adsorbed water and the zeolite at their optimized adsorption configurations, that is, $\Delta\rho = \rho(\text{water/HZSM-5}) - \rho(\text{water}) - \rho(\text{HZSM-5})$.

2.3 Results and Discussion

2.3.1 ZSM-5 Characterization

As previously discussed, the unit cell of ZSM-5 has 96 tetrahedral sites (T sites) of silicon and 192 oxygen atoms.[53] The pore network is composed of two types of interconnected perpendicular channels, one of them straight and the other sinusoidal, weaving perpendicularly to each other. Of the 96 T sites, there are 12 symmetrically distinguishable T site locations that can be occupied by Al (see Figure 5). In addition, each of these T sites has 4 different neighboring oxygen atoms making a total of 48 different configurations for isolated BAS[5]. This complexity can be simplified by focusing

on the most stable and physically accessible sites around the channel intersection, as can be seen in many prior studies.[10, 37]
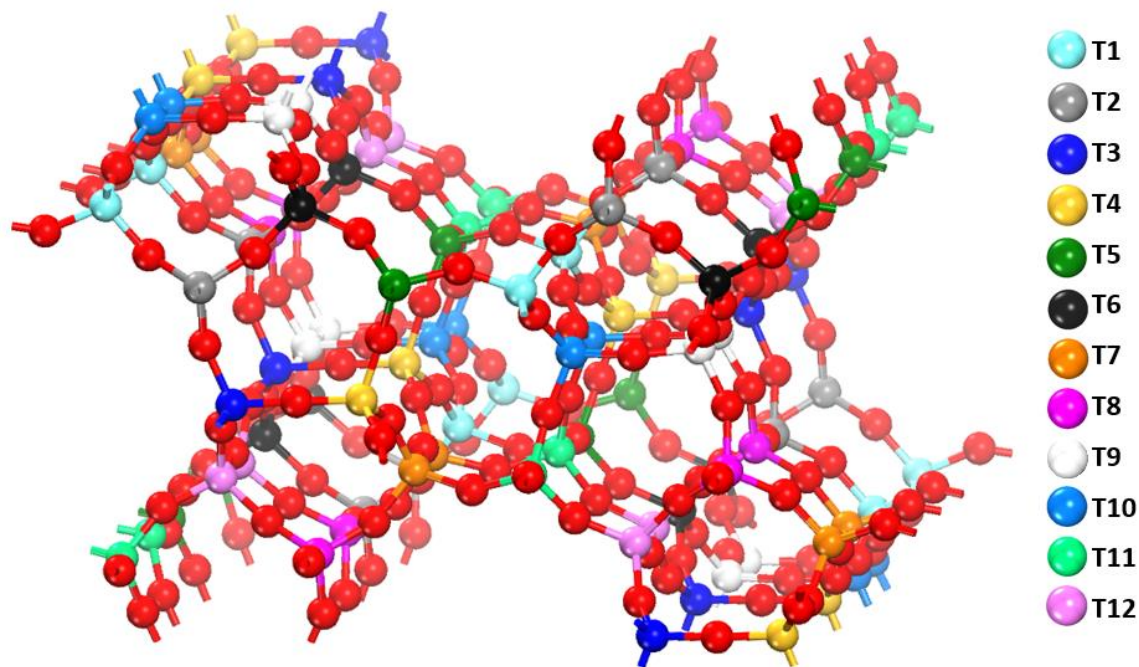
Figure 5: Atomic structure of the ZSM-5 unit cell with the 12 distinguishable T sites color-coded.

The T site chosen for Al substitution can have a large impact on the calculation results.[54] Also, local confinement must be carefully considered.[5, 55, 56] In an effort to reduce excess computational expense, prior theoretical studies have often been focused on specific T site locations, the most common being sites T7 and T12. This selection has been based on the highest accessibility to reactants (e.g. T12) or the highest stability, relative to the other sites when substituted (e.g. T7).[5] The distribution of Al at different T sites is mostly driven by nucleation and growth kinetics during the synthesis[19], and more than 10 different framework T sites have been reported in H-ZSM5 samples[57]. The site T7 and T10 has been shown in previous studies as generally being the most highly

populated positions.[58-61] The choice of the organic templates in synthesis plays a large role.[5, 62] One of the more common agents used for this synthesis is tetrapropylammonium (TPA) and has been shown to result in aluminum placement primarily on the channel intersections, taking advantage of the aforementioned site accessibility.[62]

In this study, the T7 site is the starting point, and the conclusion is likely generally true for all T sites as discussed below. In order to capture the effects of BAS proximity, two T sites were substituted with aluminum, one always being the T7 site, and categorized by the number of T sites that separate them, labeled as D1-D4 (see Figure 6), which is the same as notation Al-O-(Si-O)$_x$-Al-O with x between 0 and 3. The BAS separation was then defined as the distance that separates the two oxygen atoms that have a bonded proton, following the path around the channel.
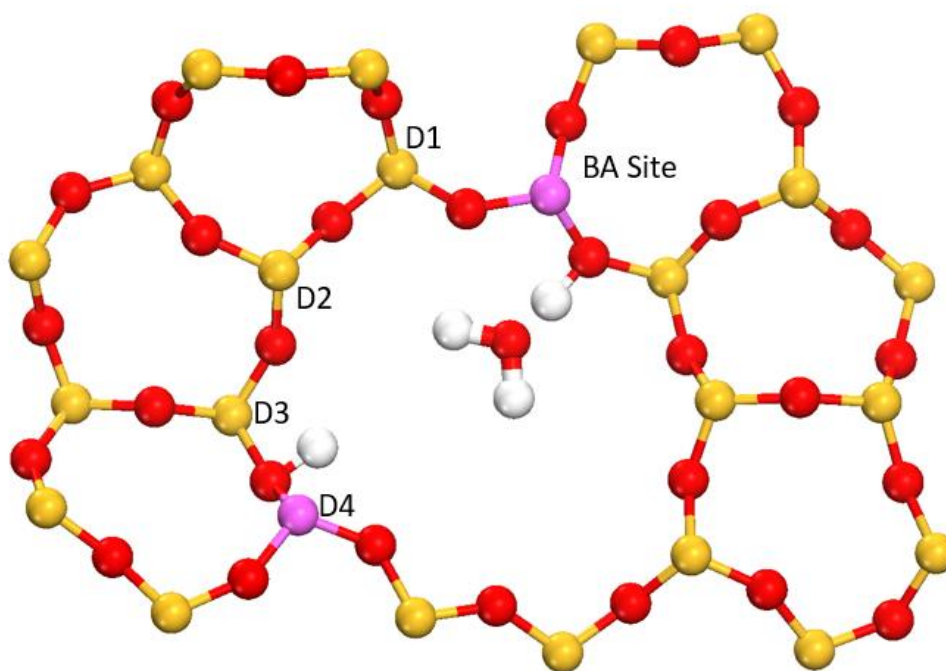
Figure 6: HZSM-5 crystal layer with labels showing the terminology used in describing site separation. A water molecule is positioned close a T7 site in all the calculations, while the second BAS is positioned with varied distance from the T7 site. The Si, O, Al, H are colored yellow, red, purple and white, respectively.

Water was then used as a probe to compare local activity, DFT calculations were used to examine properties of interest to acid catalysis[63], which may be considered an indicator for acid strength, which determines the activity and selectivity in zeolite-catalyzed reactions[63, 64]. Improved understanding of how water molecules adsorb in zeolites with densely populated acid sites may also help to improve the stability of the zeolite in a liquid phase and its catalytic performance.[17, 56, 65]

The configuration of a single isolated BAS site was the first to be investigated. The same as for previous studies, site T7 was among the most stable sites for Al substitutions as can be seen in Table 1.[5] The stability also varies when the proton is positioned at different oxygen. Table 2 shows the sensitivity of energy towards proton position around site T7. The importance of using the most stable site is debated, since experimentally it is shown that the site distribution is dependent on synthesis conditions, but for reasons of calculation consistency and reproducibility, the stability of the chosen substitutions is still considered nonetheless.

Table 1: Relative stability calculations between the 12 possible T sites. The energy of the most stable site is set to zero and only the relative energies are shown.

Site	Energy (eV)	Relative Stability	Literature[5]
T1	-2301.6132	0.18	0.26
T2	-2301.5711	0.22	0.28
T3	-2301.6711	0.12	0.26
T4	-2301.7811	0.01	0.1
T5	-2301.6351	0.16	0.32
T6	-2301.6195	0.17	0.35
T7	-2301.7538	0.04	0
T8	**-2301.7932**	**0.00**	**0.21**
T9	-2301.5562	0.24	0.38
T10	-2301.5828	0.21	0.17
T11	-2301.5527	0.24	0.26
T12	-2301.6955	0.10	0.2

Table 2: Relative stability calculations between possible configurations of site T7. The first number describes which T site is substituted with Al and the second describes the neighboring T site that the protonated oxygen is bisecting. The energy of the most stable site is set to zero and only the relative energies are shown.

Site	Location	Hydrogen Direction	Stability (eV)[b]
7-4	Intersection	Sinusoidal Channel	0.057
7-4	Intersection	Straight Channel	0.066
7-7	Intersection	Sinusoidal Channel	0.208
7-7	Intersection	Straight Channel	0.203
7-8	Intersection	Sinusoidal Channel	0
7-8	Intersection	Straight Channel	0.011
7-11	Intersection	Sinusoidal Channel	0.272
7-11	Intersection	Straight Channel	Inaccessible

Protonating site T7-8 is the most stable with differences between the directionality of the proton being negligible. Site T7-11 is the only site found to be inaccessible to adsorbates due to steric hindrance. The stability differences between protonating sites are found to be significant enough to warrant computing the most stable proton configuration for simulations but overall less significant than the choice of initial T site. The energy difference between these different configurations is about 1-10 times k_BT at room temperature (0.026 eV), where k_B is the Boltzmann constant, and suggests that at room temperature, the proton may hop between a couple different sites.[9] Thus, the proton and the molecular adsorption at the proton can be quite dynamic during reactions.

2.3.2 Heat of Adsorption Calculations

Note the distribution of Al at different T sites is mostly driven by nucleation and growth kinetics during the synthesis.[19] In the following calculations are restricted to the most stable calculated configuration, that is, Al is located at the T7 position and proton is bonded to oxygen between T7 and T8 (Al-O-Si), and vary the other Al site between different positions. The advantage of this self-restriction is two folds: this reduces the total number possibilities of Al-O-$(Si-O)_x$-Al pair configurations; and, as detailed below, when water was used as a molecular probe, the water always positioned to form a H-bond with the proton bonded to oxygen between T7 and T8, and in this way, the entropy change for water adsorption remains almost constant when the spacing between the two BAS is changed.

When two BAS are introduced into the H-ZSM5 framework, the focus is on Al configurations that allow the protons face into the same channel of H-ZSM5 and can

cooperate with each other for coordination[19], but some other configurations have also been included to compare with x up to 5 in the Al-O-(Si-O)$_x$-Al sequences .

Figure 7 shows the calculated heat of adsorption for water. The adsorption is shown to be significantly stronger as the site separation is smaller. In D1 configuration Al-O-(Si-O)$_0$-Al, in which the spacing between the two BAS is about 3.5 Å, the heat of water adsorption is about two times the value of D3-D6 configurations corresponding to Al-O-(Si-O)$_x$-Al with x between 2 and 5. The D2 configuration, which is Al-O-(Si-O)$_1$-Al, also shows stronger interaction than D3-D6 by about 40 kJ/mol. Once the spacing between the two BAS is equal to or large than 2 (Si-O) units, the adsorption energy flattens out and become similar to the adsorption of water at a single isolated BAS as would be expected as the two sites are no longer electronically see each other to a significant margin. This data is in agreement with experimental results, where at a very high Si/Al ratio equal to 250 (~1 substituted Al per 3 unit cells), the adsorption energy of water was found to be -0.78 eV, while at a low Si/Al ratio of 38 (~3 substitutions per unit cell), the adsorption energy was found to be -1.17 eV[15, 66], which is close to the calculated adsorption of water when two BAS are located in close proximity (D1 and D2). The hybrid functional HSE calculations do not significantly change the adsorption energy calculations as shown in Figure 7, However, the PBE and HSE calculations differ significantly in the stability calculations to a significant margin (see Figure 10). Due to significant stability differences and breaking the Loewenstein rule that states no Al atoms should occupy adjacent T sites, D1 should be considered as an extreme case unlikely to form under regular zeolite synthesis.[67]
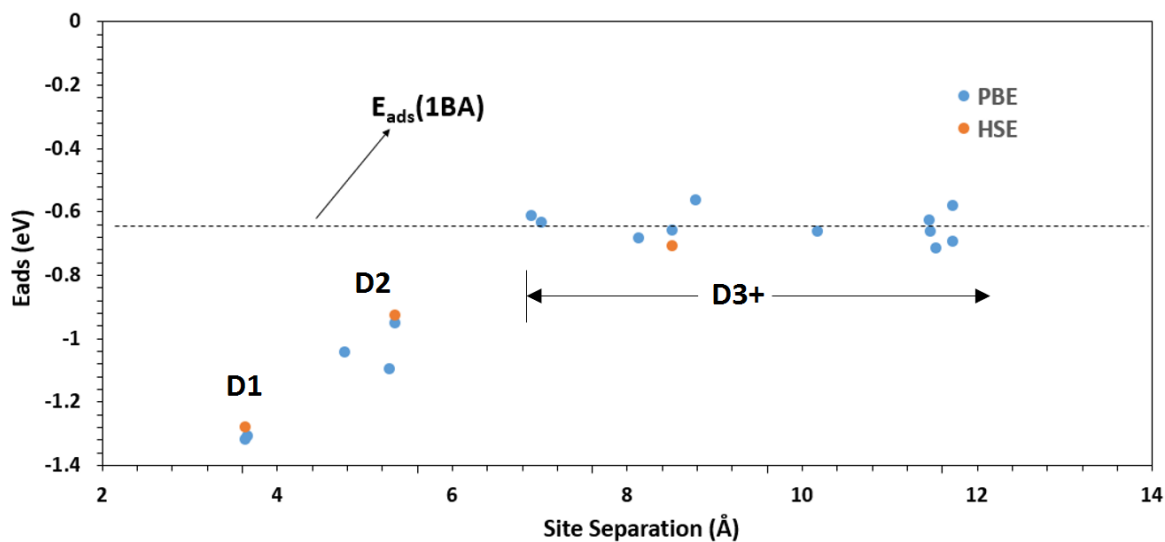
Figure 7: Calculated water adsorption energies plotted as a function of separation between two BAS. The values are also compared to the average found for the case of 1 BAS (dashed line). Hybrid functional HSE calculations over a select few points are shown in orange.

To understand the physical reason behind this significantly enhanced water adsorption as the site separation decreases, the change in charge densities caused by water adsorption at the BA sites was examined (Figure 8). At site separation D1, the water is shown to be strongly protonated and form a H_3O^+, which is adsorbed via two H-bonds to both the original T7-O-T8 and another oxygen atom of the second BAS (Figure 8C). The adsorption-induced large depletion of the electron density around the H_3O shows a localization of positive charge on the water, now a hydronium. This finding shows that thermodynamically the proton prefers to be localized at the water molecule forming H_3O^+ rather than the oxygen atom bonded to wthe substituted Al center. It is expected that a large number of water molecules can further enhance the deprotonation of the BAS and form a more mobile proton within the water network because of the increased dielectric screening. This deprotonation is in line with recent work of dehydration of cyclohexanol

23

in liquid phase using solid acids as the catalysts.[17] Hexane was also tested as an example

of non-polar molecules and find negligible difference between adsorption energies of one

BAS and two BAS at D1 (Table 3). This different trend between hexane and water

adsorption in zeolite indicates important role of the polarity of the adsorbates.

Table 3: Hexane adsorption energy calculations between the 1 BAS and D1 BAS.

Site	Zeolite Energy (eV)	Zeolite with Hexane (eV)	Adsorption E (eV)
B1. T7-8	-2301.55	-2409.47	-1.13
B1. T7-4	-2301.56	-2409.51	-1.16
B1. T7-7	-2301.42	-2409.48	-1.07
D1. T78-9	-2303.68	-2411.72	-1.15
D1. T78-2	-2303.67	-2411.54	-1.07
D1. T78-12	-2303.55	-2411.47	-1.18

2.3.3 Charge Density Calculations

By increasing the site separation to D2 (Figure 8B), in which one (Si-O) unit

separates the two sites, the H_3O^+ species doesn't form, at least for the single water studied

in this case. Instead, the water adsorbs at the T7 BAS forming a H-bond with an oxygen

atom at the second BAS. This cooperation between the two BAS enhances the water

adsorption by almost half eV as compared to the single isolated case (dashed line in

Figure 8).

At distances larger than that of D3, in which two (Si-O) units separate the two

BAS, water adsorbs at the T7 BAS with a single H-bond formed. Note water is one of the

smallest molecules to be used for probing the local activity. It is expected that, if a large

probing molecule is used, even when two BAS are further apart from each other,

adsorption of the probing molecule may still be enhanced. Indeed, recent experiments suggested enhanced adsorption of n-hexane and acetone in low Si/Al samples (Si/Al=16), which was attributed to increased polarization by more than one BAS in HZSM-5.[16]
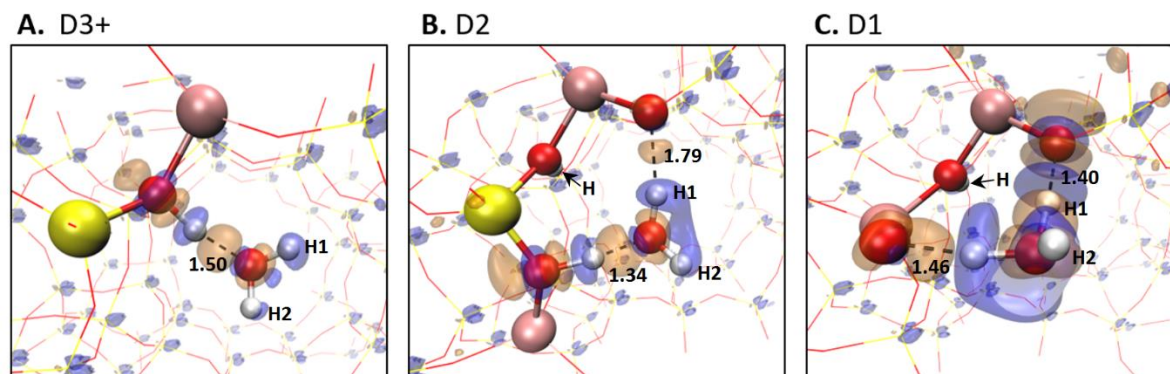
Figure 8: Adsorption-induced changes in electron densities are shown with the orange portions being areas of electron density accumulation and blue areas of electron density depletion. The isosurface used to plot the charge density difference is ± 0.03 e Å^{-3}.

Figure 8 A-C also suggests different amounts of charge transfer between water the HZSM-5 framework. The charge transfer is more pronounced when water interacts with two BAS. In all situations the hydrogen atoms on the original water molecule are shown to lose electrons and become more positively charged. Bader charge analysis was used[68], through which the values for the charge difference resulting from reaction was obtained and listed in Table 4. In every situation, the two hydrogen atoms of the water lost electrons while oxygen gain electrons, indicating enhanced polarization upon adsorption. As the proximity reaches D2 and D1, that charge difference is nearly doubled and tripled as compared to D3, respectively. Note that there are different ways to define exact number of the electron population at an atom in the literature, which may give different numbers but the trend should remain.

Table 4: **Bader charge analysis. The first hydrogen H1 refers to the internal hydrogen of the water that bonds with a neighboring oxygen. The second hydrogen H2 refers to the hydrogen that points towards the pore. H1 and H2 are labelled in Figure 8 for reference.**

Site	E_{ads} (ev)	Charge difference (H1-H2-O)[a]		
D1	-1.31	-0.14	-0.13	0.14
D2	-1.09	-0.12	-0.07	0.08
D3 & D4	-0.66	-0.05	-0.03	0.03

2.3.4 Hybrid Functional Analysis

All these calculations suggest enhanced water adsorption when the two BAS are in the close proximity with x is equal to or smaller than 1 in Al-O-(Si-O)$_x$-Al. The energy difference was calculated for two acid sites within a unit cell of H-ZSM5 when varying the separation between two BAS. It is intriguing to notice that the calculations performed using the DFT-PBE functional don't show significant variation of the energy when changing the Al-Al distance within a pair (Figure 10A), indicating a relatively random distribution of isolated and paired acid sites. This trend is rather counterintuitive, because one would expect electrostatic repulsion between the charges localized at the two acid sites should become pronounced when two BAS are in the close proximity and cause significant repulsion between the two sites.

It is well known that charge delocalization error exists when semi-local functional, such as PBE, is used for calculations of charged species.[50] Indeed, when HSE hybrid functional is used, a drastic change of the profile is obtained (Figure 10B), in which a large energy cost is observed when the separation between the two sites is within two (Si-O) units. The data was fitted to have the energy reduce (becomes more stable) linearly as a function of 1/r (Figure 9), which should be expected as the electrostatic

interaction dictates the thermal stability. The basic for this can be seen in the equation for

Coulomb interaction explained in Chapter 1 while discussing the groundwork of DFT.
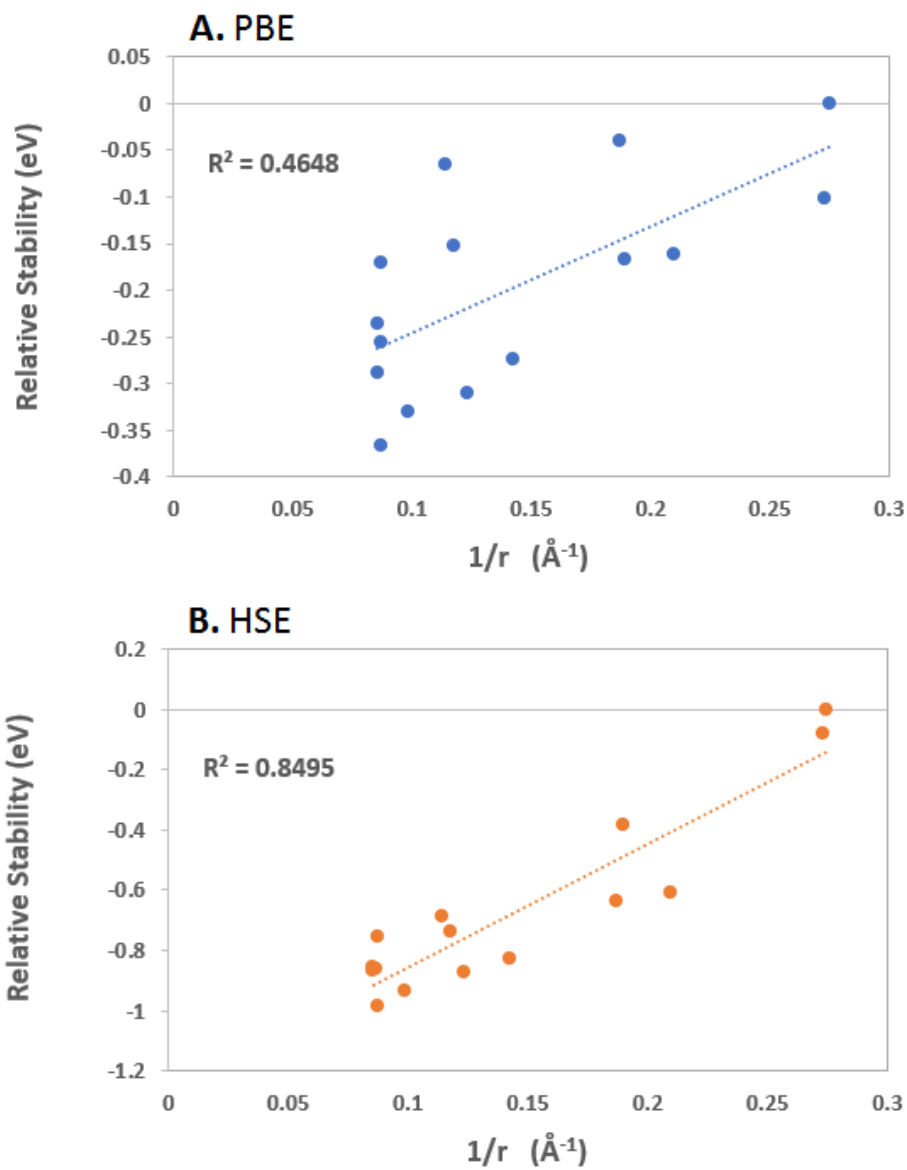
Figure 9: Comparison between the ability of PBE and HSE functionals to calculate the stability of the two-site HZSM-5 as a function of site separation.
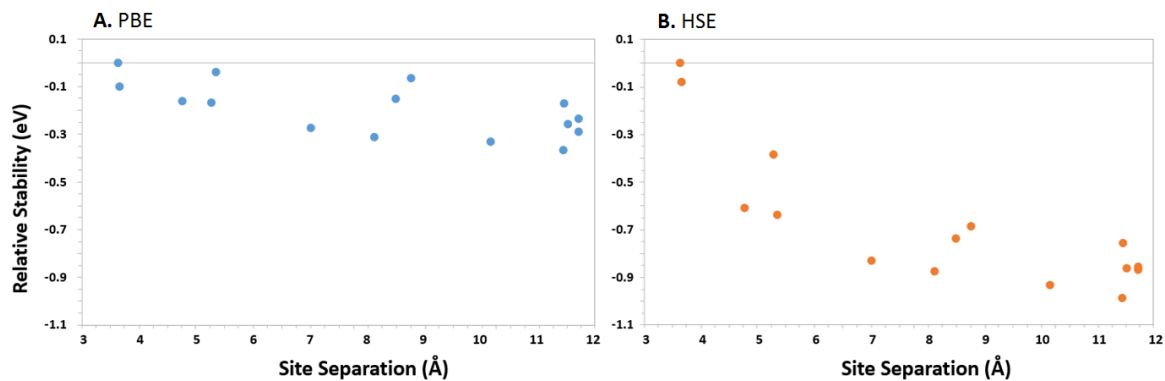
Figure 10: Energy difference between two BAS configurations as a function of the distance between the two sites. Both the semi-local PBE functional and HSE hybrid functional are used, which show different variation of total energies between configurations. In (A) and (B), the total energy of the least stable configuration is set to zero, so only the relative energies are plotted in the figure.

This energy penalty for forming these pairs suggests that the specific D1 and D2 structures are not as thermodynamically stable as if the sites are separated. However, it is noted the D2 Al-pair Al-O-(Si-O)$_1$-Al is populated with low possibility in most Si-rich H-ZSM5 samples[57], while in Al-rich frameworks (Si/Al ~ 8), predominantly Al-O-(Si-O)$_1$-Al sequences have been formed[19]. The thermodynamic energy penalty for forming these pairs shown in the DFT calculations thus suggests that the formation of close Al pairs is kinetically controlled in previous experiments by varying the structure-directing agents.[20-22] It should be pointed out that the water adsorption energy is insensitive to the functional used in the calculations (Figure 3), which may be caused by cancellation of errors when calculating the systems with and without water adsorption.

2.4 Conclusions

The effects of location and density of BAS on water adsorption in HZSM-5 was studied using DFT calculations. Adsorption energy of water grows significantly as the separation between BAS decreases because of interaction of water with two acid sites in close proximity (zero or one Si-O unit between the T sites). The water is polarized by both sites leading to the enhanced adsorption, which is evidenced by the directional charge transfer. These results suggest that for a molecular reaction in HZSM-5, and probably other zeolites as well, adjacent acid sites, which exist in low Si/Al samples, may play a role in determining the molecular adsorption and reaction. The enhanced water adsorption also suggests that the acid sites in the proximity may serve as nucleation centers for water wetting the surface. In addition, it is expected the proton delocalization from the zeolite framework into water may be more pronounced when a large water cluster or an aqueous phase is present in the system. This concept will be examined in Chapter 3. On top of that, both the enhanced polarization and proton delocalization may affect activity and selectivity for zeolite-catalyzed reactions. This will be investigated in Chapter 4.

Chapter 3: Behavior of Water Clusters on Zeolite Acid Sites

3.1 Introduction

One of the important elements of the results of Dr. Gumidyala[14] and Chen et al.[13] is that water had to be present to some degree for this enhancement to take place. Looking through the literature gives some ideas of what might be going on. As is shown by Vjunov et al.[17], at ambient conditions water forms a cluster around the acid site and the protons are present as hydrated hydronium ions that are ion-paired to the zeolite. This can be seen in DFT simulations as well as in IR spectra taken at different temperatures. The DFT-optimized structures seem to indicate that the proton enters the water cluster when there are two or more water molecules in the cluster. The study proved the existence of these clusters by comparing experimental IR spectra taken at various temperatures with the IR frequencies calculated using the DFT optimized structures for different concentrations of water in the zeolite pores. At 30 °C, approximately 5 of the predicted bands at 3615, 3750, 3345, 3130, and 2955 cm^{-1} for structure V ($H_{11}O_5^+$) are observed in the experimental spectrum at similar frequencies. Between 70°C and 120°C there is a broad shoulder near 3400 cm^{-1} and around 1700 cm^{-1} that are consistent with smaller $H_7O_3^+$ or $H_9O_4^+$ clusters.[17]

For near ambient reactions over zeolite, the formation of water clusters could be the key to reaction enhancement, possibly stabilizing charge intermediate species or making the protons more accessible to reactants. Finding answers to these questions of water cluster enhancement will require further analysis of the subject. The approach taken by this text will be using ab initio molecular dynamics (AIMD) Simulation to better understand how water would behave at conditions such as those done in the literature.

As discussed in previously, the MFI framework consists of two types of intersecting 10- membered-ring pores. The geometry and size of these perpendicular pores differ: one type consists of straight channels with a size of 5.3×5.6 Å^2, running along the crystallographic b-axis, the other has a tortuous shape, commonly referred to as the sinusoidal channels, with a size of 5.1×5.5 Å^2 , running along the crystallographic a-axis[11]. Such differences in pore size and local environment can trigger different adsorption properties between the two types of pores. For example, it has been shown that aromatic molecules, such as p-xylene, p-dichlorobenzene, and trans-stilbene, preferentially adsorb at different locations of the framework depending not only on the adsorbate nature but also on the adsorbate loading.[11]

In one study done by Kubarev et al.[11] it was claimed that solvents appear to selectively absorb in one of the two channels based on the polarity of the solvent. It shows that differences in solvent and reagent polarity can be employed to steer the catalytic activity toward the straight or sinusoidal pores in HZSM-5. This effect was attributed to the intrinsic presence of silanol defects. CLS microscopy in combination with furfuryl alcohol oligomerization as probe reaction shows that this acid catalyzed reaction preferentially occurs in the straight pores of H-ZSM-5 crystals if water is used as the solvent and in the sinusoidal pores if more apolar 1,4-dioxane or 2-butanone are used.

Strangely enough, even without silanol defects the AIMD simulations of this chapter were showing that water would preferentially locate itself in the sinusoidal channels, even when water near saturation. Since there were no silanol defects to attribute this to, the conclusion drawn here was that hydrogen bonding between the water was greater in the sinusoidal channel and intersection as compared to the straight channel.

3.1.1 Ab initio Molecular Dynamics (AIMD) Simulation

As already discussed the primary calculation technique use in this chapter are ab initio molecular dynamics simulation, or AIMD. The goal of AIMD is quite simple: given a system of particles, all potential forces involved, and their positions in space and initial conditions, integrate Newton's equations of motion to compute future positions, velocities, and forces of each particle for as long as the computational resources allow.[69] This algorithm can be summarized in four basic steps. First, input conditions of potential forces, positions, and velocities are given. Second, the resulting forces on an atom are calculated based on the equations used by the specific simulation method. Third, the configuration is updated to the next time step based on those forces. Finally, the new conditions of positions, velocities, energies, ect. are output from that new configuration. Steps 2-4 are repeated until the number of steps has been satisfied or the calculation time has been reached.

AIMD simulations allow for a bridge between theory and experiment; they fill in the gaps that experiment cannot easily access and vice versa. It is challenging for experimentalists to track movements of a single molecule on the picosecond scale but with AIMD it is possible. Essentially the molecules take the path of least resistance the same way as they would in reality and this gives insight into how the molecule would behave in real world situations. The AIMD simulations undertaken by this project are not too complicated. Starting with a ZSM-5 framework the same as Chapter 2 differing amounts of water were added and the behavior in the pores and BAS interactions were analyzed.

3.1.2 *Explicit vs Implicit Solvation*

One concept touched upon in this chapter but investigated more in depth in Chapter 4 is the idea of simplifying the calculation by implicitly calculating the solvation energy. Conceptually, it is very easy to see why this would be easier to calculate, especially for dozens of water molecules. Rather than spend the calculation time for all of the separate water molecules to orient themselves correctly, a continuous polarizable field can be applied using the bulk dielectric constant of water.
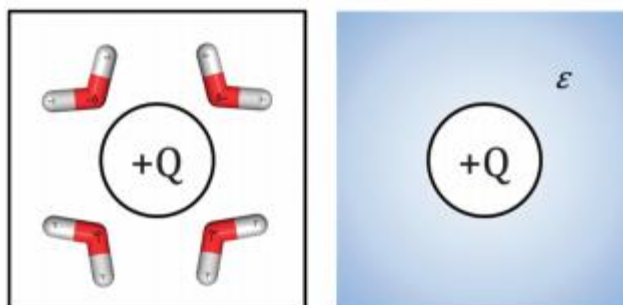
Figure 11: For explicit solvation, water molecules reorient themselves to preferentially point the negative end of their dipole towards the positive solute charge (left). For implicit solvation, the system can be modelled with a continuous polarisable field (right). This graphic was taken from Skyner et al.[70]

3.2 Computational Methods

For the most part the calculations are the same as those done in Chapter 2. Calculations based on density functional theory (DFT) were carried out using the VASP (Vienna ab initio simulation) package.[43] The PBE generalized gradient approximation (GGA) exchange-correlation potential[44] was used, and the electron-core interactions were treated in the projector augmented wave method[45, 46]. The van der Waals interaction was considered through DFT-D3 semi-empirical methods via a pairwise force field.[47, 48]

All the calculations were performed using a ZSM-5 unit cell including 96 Si and 192 O atoms. The structure of the unit cell was taken from an experimental work (a =

20.078 Å; b = 19.894 Å; c = 13.372 Å)[53] and fixed during the calculation. Where this differs from chapter 2 is that in addition to the unit cell, differing amounts of water molecules were added to the pores. AIMD simulations with two BAS in the D2 configuration were done with water contents of 6, 23, and 30 water molecules. 6 water molecules in order to emulate the results of Vjunov et al.[17], 23 water molecules as a predicted amount by Olson et al.[66], and then 30 water molecules from a personal calculation of a saturated ZSM-5 pore. In addition, 37 water was added with no BAS in order to examine solvent channel preferences.[11]

AIMD Simulations were set to 4 minimum electronic self-consistency steps and temperature is set to 320K. Each separate configuration was run for a total of 10ps, aside from the 30-water case because the 30 water molecules proved to not be enough to fully saturate the zeolite pore. Results shown are visualized using the software Visual Molecular Dynamics (VMD).[71]

3.3 Results and Discussion

3.3.1 Water Cluster Interaction with BAS

It is clear from Dr. Gumidyala's results[14] that water has a vital role to play in the enhancement, but it is less clear what that role is. As mentioned in this chapter's intro, Vjunov et al.[17] had an intriguing finding where water clusters would deprotonate a BAS and distribute the charge throughout the cluster via hydrogen bonds. In pursuing this theory, AIMD calculations were chosen as a way to observe how process occurs in real time and how quickly. A temperature of 320K was chosen as a near ambient condition as was in Vjunov et al.[17]. For the first AIMD simulation, the same size of the water cluster was used. But as an additional twist on that experiment, the optimal D2 configuration as detailed in Chapter 2 was used rather than just a single BAS. The AIMD simulation was run to 10ps but after 3ps the cluster is mostly stable, simply trading the proton between water molecules. These results can be seen in Figure 13 and 14.

Figure 12: D2 BAS with 6 water, including initial configuration and 1ps snapshots of the AIMD simulation. The dashed green lines indicate hydrogen bonds and the protons that become hydronium are labelled.

Figure 13: D2 BAS with 6 water, including 2ps and 3ps snapshots of the AIMD simulation. The dashed green lines indicate hydrogen bonds and the protons that become hydronium are labelled. Note both protons have entered the cluster at 3ps but the second is held tightly to the acid sites.

Looking at these one by one, Figure 13A shows the beginning of the AIMD simulation. These water molecules were placed by hand so they aren't realistically arranged at this stage. By 1ps in 13B, one of the BAS protons has already detached and entered the water cluster. This occurred much quicker than expected, implying that the proton highly prefers the hydronium form. This helps put in perspective why water is often such a problem for competitive absorption and killing sites in zeolites.[72]

The next figure shows the further stripping of these acid sites. At 2ps in figure 14C, the first proton has begun to progress further away from the BAS and into the cluster, and the second BAS is beginning to form a second hydronium ion. By 3ps in 14D, the first proton is held two water molecules away from a BAS and the second has completely detached into a hydronium cooperatively absorbed similar to Chapter 2.

The results for 6 water molecules was interesting so from there it was decided to mostly fill the pore to the same amount as that in an article from Lercher's group, 23 water molecules in total.[9] These results can be seen in Figure 15 and 16. The first thing to notice for the larger water cluster is how much faster the timescale is. Deprotonation happens immediately, and the protons drift further away from the acid sites as for the 6 water cluster. The only thing that is similar is that after 3ps the cluster is mostly stable in how far away from the BAS the protons go.

Figure 15A is once again simply the initial starting point of the AIMD simulation. 15B is at a similar point as 13B was but it is important to note that it reached this point 0.1ps, a tenth of the time it took for the 6 water cluster. With this many water molecules it is significantly harder to tell is going on but behind the first layer of water the hydronium ion can be seen. At this point the other BAS proton is still firmly intact.
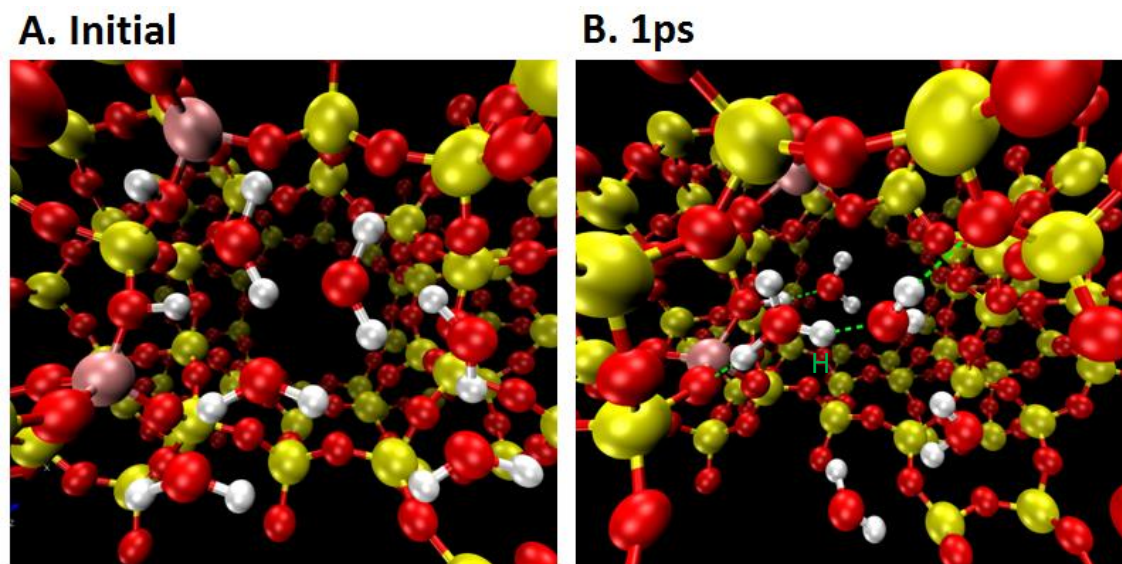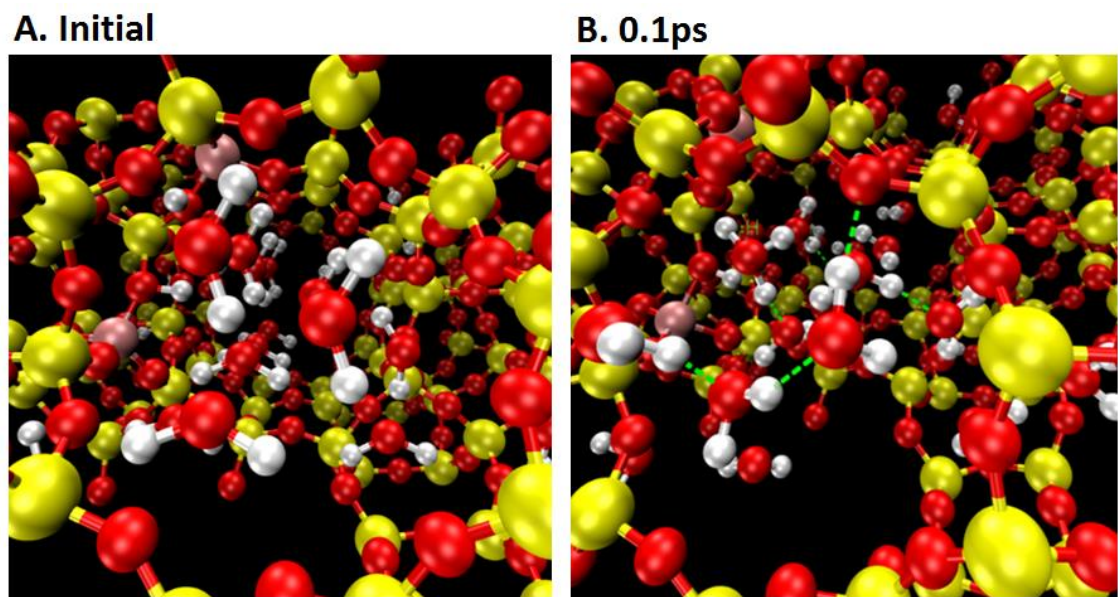

Figure 14: D2 BAS with 23 water, including initial configuration and 0.1ps snapshots of the AIMD simulation. The dashed green lines indicate hydrogen bonds and the protons that become hydronium are labelled. We do notice that at this short time thermal equilibrium within the system has not been reached.

As can be seen by Figure 16A, by 0.2ps the first proton is now well stripped from the BAS, a full 2 to 3 water molecules away. Further in the back it can be seen that the other water is beginning to strip away as well. Shortly after it does strip but the next image 16D fast forwards to 3ps, at which point the AIMD simulation is fairly stable. At this point a well-developed cluster has collected, holding both the protons from the acid sites 3 full water molecules away. There might be brief moments in future parts of the AIMD simulation shows them 4 water molecules away but the proton quickly returns to around a 3 molecule distance.
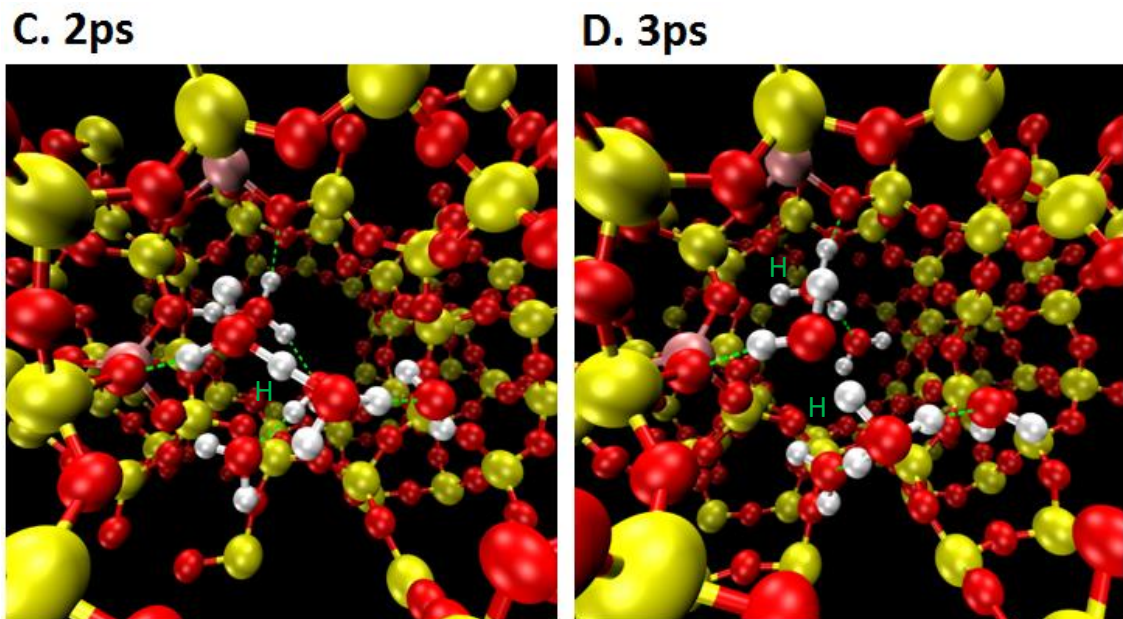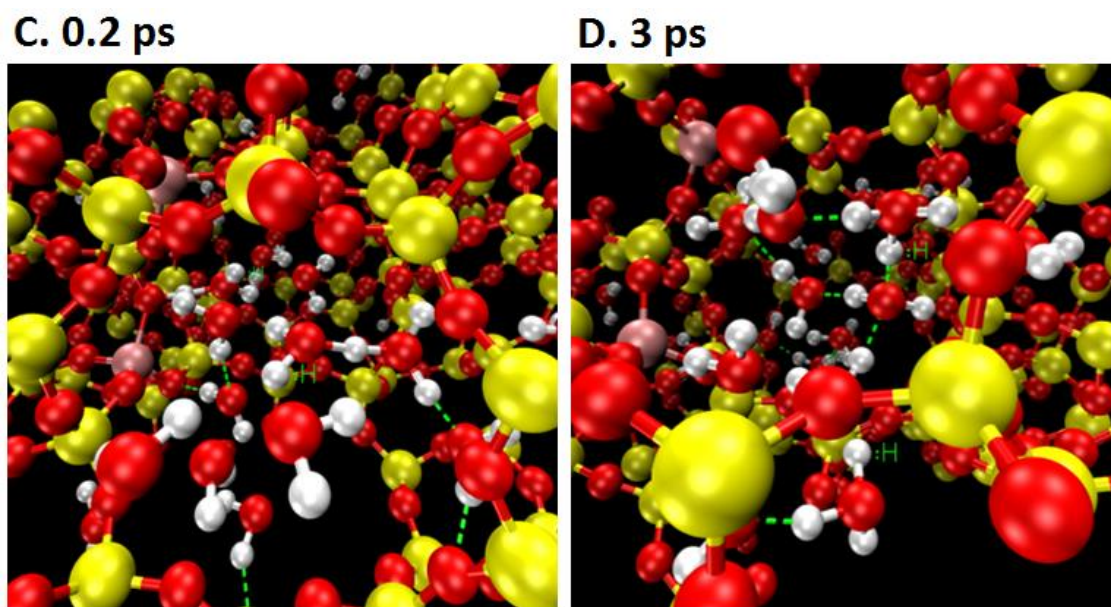

Figure 15: D2 BAS with 23 water, including 0.2ps and 3ps snapshots of the AIMD simulation. The dashed green lines indicate hydrogen bonds and the protons that become hydronium are labelled.

While intriguing it is not altogether clear what this might mean for reaction enhancement. If anything this shows how the acid might be weakened. The takeaway for improving the reaction is the stabilization effect of the water cluster. What might be bad for acid sites is good for reaction intermediates. Chapter 4 will explain further.

3.3.2 Water Preferential Channel Diffusion

An additional curiosity found during the AIMD simulations was that the water molecules were shown to selectively diffuse to the sinusoidal channels. This is seen the strongest for the partially filled pore with 23 water molecules, but all the rest of the AIMD simulations all also show it to some degree. Kubarev et al.[11] attributes this to silanol defects, but since these unit cells do not possess any, there must be some additional explanation, at the very least for water. Water follows the prediction given by that report, where polar solvents, interacting with each other through H-bonds, prefer the sinusoidal channel and nonpolar prefer the straight channel.

The AIMD simulations displaying this are shown in figures 17, 18, and 19. In all of these images, the zeolite unit cell is being viewed perpendicularly to the direction of the straight and sinusoidal channels. The straight channel runs horizontally through the center of the images, and the sinusoidal channels can be seen running vertically on the right and left sides of the images.
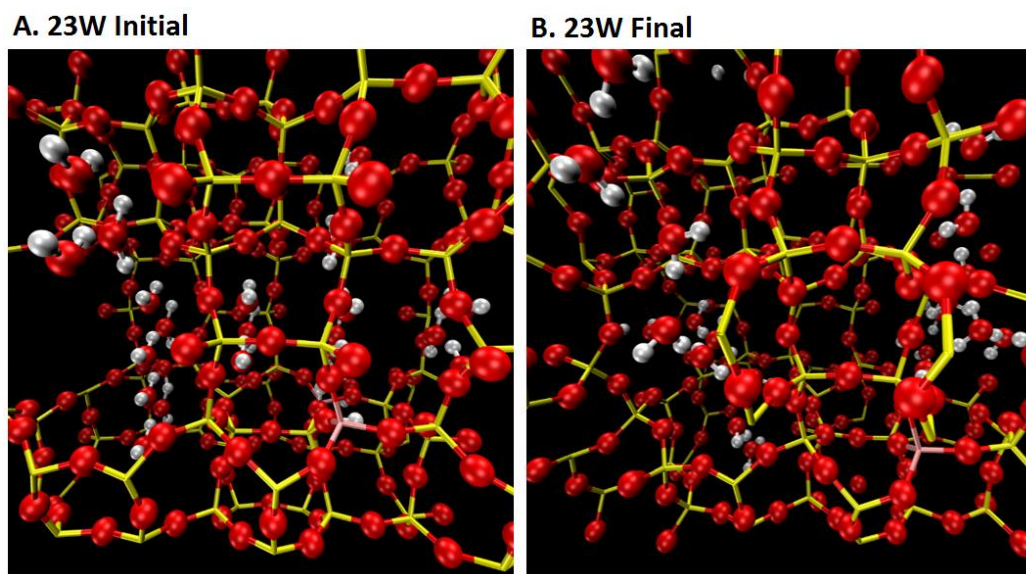
Figure 16: Beginning and end, 0ps to 10ps, of AIMD simulation for 23 water molecules in the zeolite pore, 2 BAS.
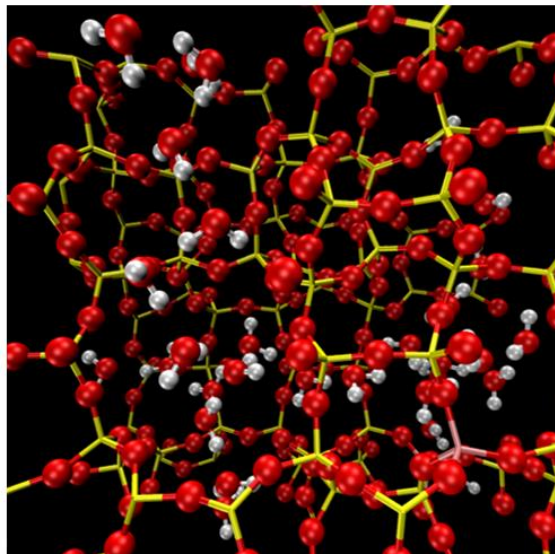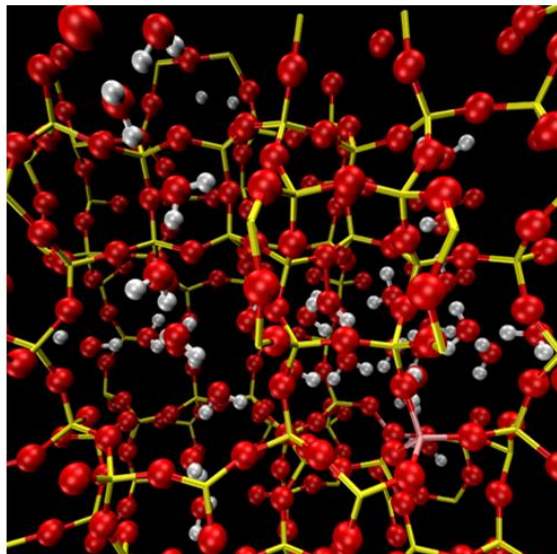
Figure 17: Beginning and end, 0ps to 10ps, of AIMD simulation for 30 water molecules in the zeolite pore, 2 BAS.
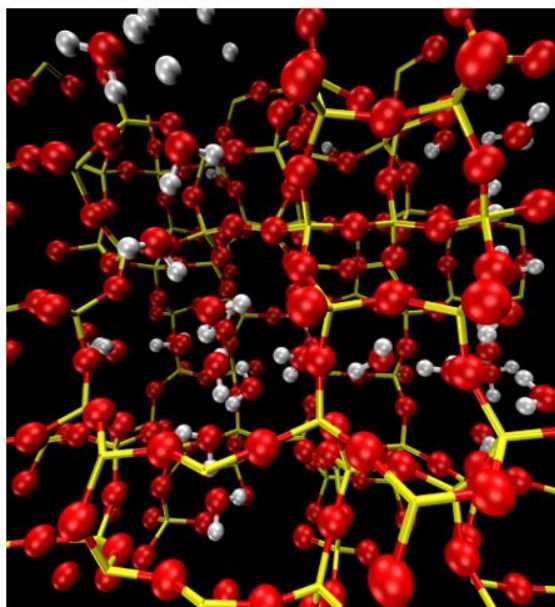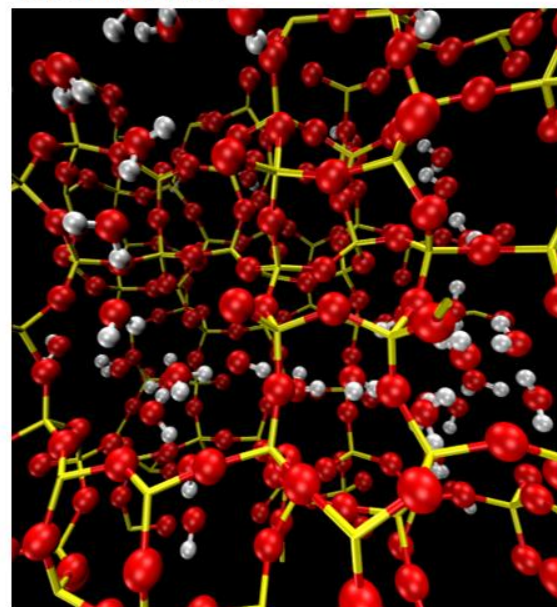
Figure 18: Beginning and end, 0ps to 10ps, of AIMD simulation for 37 water molecules in the zeolite pore, no BAS.

The reason for this preferential diffusion proposed by this study is that the sinusoidal channels allow for more hydrogen bonds to occur between water molecules, despite the pore being slightly smaller than the straight channel.[11] This can be seen visually where the angled entrances, exits, and turns of the sinusoidal channel are better suited for allowing water molecules to position themselves around each other and form more hydrogen bonds more often than that in straight channels where the water molecules essentially line up in a single row.

This visual theory was verified when VMD was used to track the number of hydrogen bonds for water molecules in the straight and sinusoidal channels in real time, seen in Figure 20. The choosing of water molecules is finicky since they are relatively mobile throughout the simulation so this mobility was minimized with the packed 37 water simulation. From this a clear difference in hydrogen bond formation can be seen.
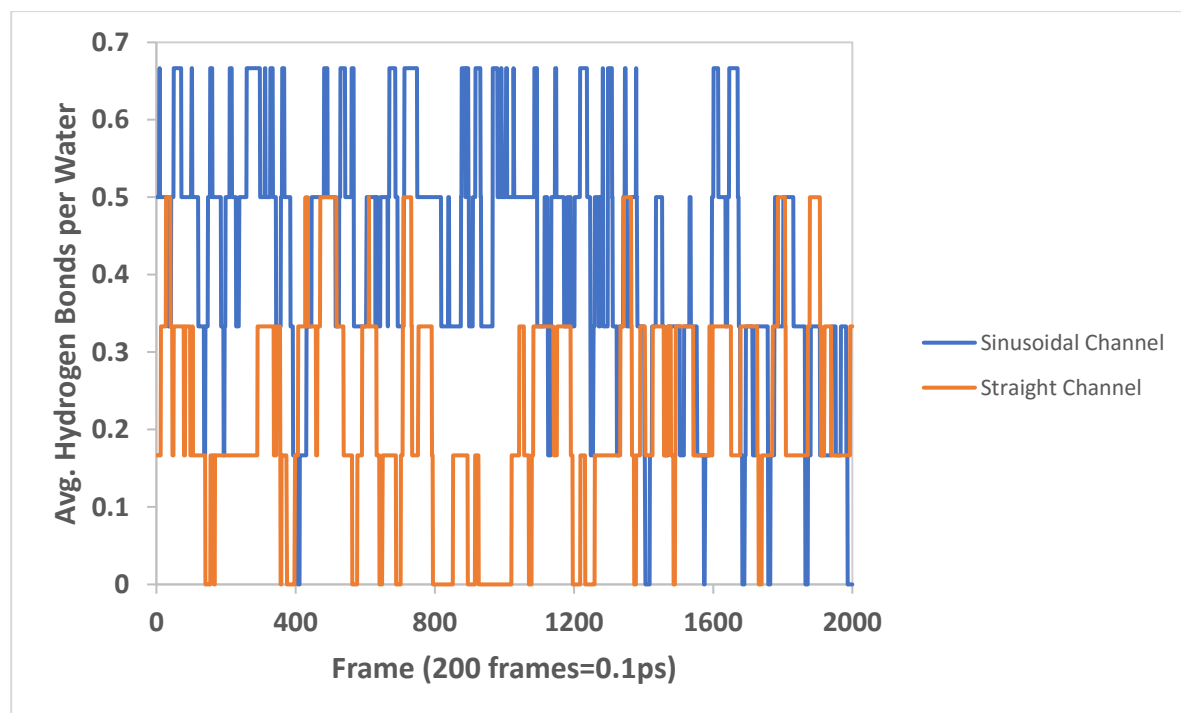
Figure 19: Average Hydrogen Bonds per Water Molecule for both the straight and sinusoidal channel with 37W per unit cell.

3.4 Conclusions

The effects of water cluster interaction with BAS and preferential solvent diffusion in HZSM-5 was studied using DFT AIMD simulations. Water clusters were shown to be highly preferential locations for protons to be rather than the BAS of zeolites. This demonstrated the strong stripping ability of water and the power of stabilizing charged species in water clusters. From this water clusters can be expected to competitively absorb on acid sites and are likely to be to the detriment of zeolite catalyzed reactions under normal circumstances. However, there is still potential for the stabilization power of water clusters to have some benefit. This is shown in Chapter 4.

In addition, water was shown to strongly selectively diffuse into the sinusoidal channel over the straight channel. This occurred for every AIMD simulation but was particularly evident for cases in which the pore was only partially filled such as with the 6 and 23 water molecule AIMD simulations. It is theorized that for water at least, the shape of the sinusoidal channel is better suited for the positioning of hydrogen bonds. The additional bonds lower the energy and makes the sinusoidal channel energetically the better place for water molecules to be located.

Chapter 4: Enhancement of Hexane Cracking from Water Clusters and Polarization

4.1 Introduction

When it came time to choose a reaction to put theories of water enhancement to the test, protolytic hexane cracking was chosen. This was done for a multitude of reasons. First and most importantly, hexane cracking was the reaction analyzed by Dr. Gumidyala.[14] Secondly, a relatively simple reaction path was found in the literature by Boronat et al.[18]. Simplicity is very beneficial when calculating barriers as the nudged elastic band (NEB) method used is prone to fail or create wildly unstable intermediates for overly complicated mechanisms. This path can be seen below in Figure 13. The only barrier focused on is that of the protonating step for the center carbon-carbon bond, the one that is 67kcal/mol in this figure. The only differences being that the alkane is hexane and it is being calculated in the reverse order.
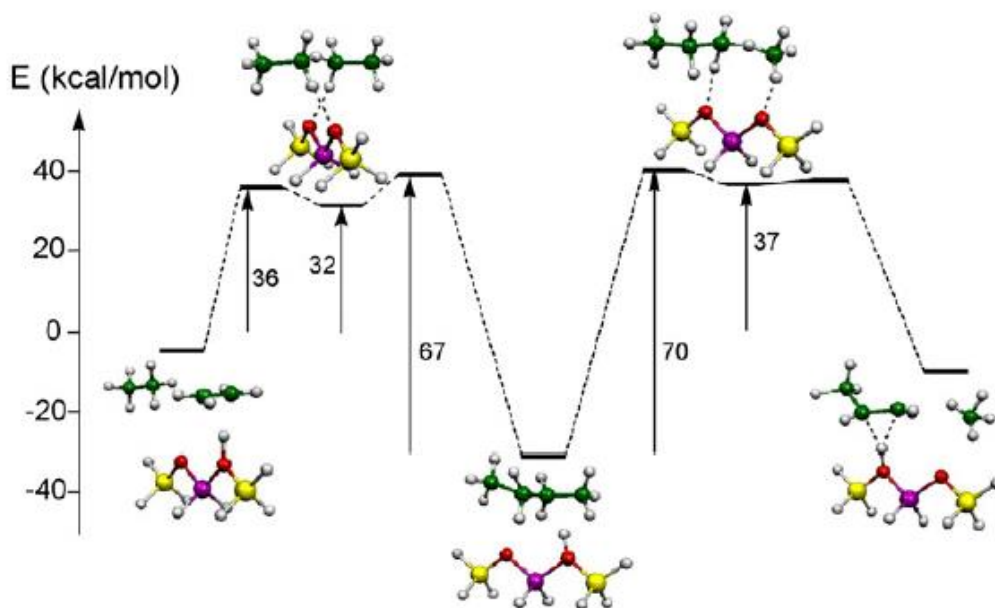
Figure 20: Calculated energy profile for the reactions of $C_4H_{11}+$ carbenium ion on a zeolite active site. This figure was taken from Boronat et al.[18]

This will be shown visually in the results of this chapter, but this mechanism starts with an absorbed alkane, protonates it at the BAS to the intermediate state of a carbonium ion, a pentavalent carbon atom, and then the molecule is split down the middle with the proton as a pseudo-transition state. This cracking could occur on any one of the carbon-carbon bonds but the center one is chosen due to it being the lowest barrier and the most likely to occur.[18, 73] In this case the goal is not modelling the entire reaction pathway that would occur for hexane cracking, but rather the goal is to single in on a highly replicable rate determining step for a cracking mechanism and to test how it is impacted by water clusters and close proximity BAS.

Alkane cracking is an important industrial process and it has been shown in numerous studies that the distribution of BAS influences the activity and selectivity.[8, 33, 34] Song et al.[16] reported that adjacent BAS in HZSM-5 shows higher adsorption energies than isolated BAS for adsorption of acetones and alkanes due to enhanced polarization, which results in increased rate for alkane cracking in HZSM-5. This is one of the theories tested. Since hexane is non-polar there won't be the same cooperative adsorption as there was for water shown in Chapter 2, but if hexane is polarized and then better stabilized from the nearby acid sites that could help to explain the enhancement.

The other theory tested is of course that the water cluster theory of Vjunov et al.[17] as discussed in chapter 3. However, since it was not altogether clear how to consistently make a barrier from a delocalized proton and whether that would even be as acidic for reaction, there had to be some other benefit that water was bringing to the table. The solution found by this text is that water served as a stabilizing element on the outside of the cracking hexane. They serve as a "flexible confinement" and could theoretically

benefit nearly any reaction, but this would require further analysis into water competitive adsorption and kinetics. Regardless, this study shows a significant lowering of the barrier for this cracking reaction. If this enhancement is stronger than the detriments of competitive adsorption, this could possibly result in a significant improvement in alkane cracking in general.

4.1.1 Nudged Elastic Band Method

The nudged elastic band (NEB) is a method for finding saddle points and minimum energy paths between known reactants and products. The method works by optimizing several intermediate images along the reaction path. Each image finds the lowest energy possible while maintaining equal spacing to neighboring images. This constrained optimization is done by adding spring forces along the band between images and by projecting out the component of the force due to the potential perpendicular to the band. The potential energy maximum along the minimum energy path, or MEP, is the saddle point energy which gives the activation energy barrier, a quantity of central importance for estimating the transition rate within harmonic transition state theory.[74] A visual representation of this process can be seen in Figure 14 on the next page.[75]

In most cases however, the images will not optimize directly to the saddle point so additional images must be run in between the two highest energy images. For this reason, NEB calculations can become very computationally expensive very quickly if the saddle point is not found. This study instead only generates one NEB calculation for each barrier from images created in the software Virtual NanoLab and opts to calculate the saddle point from the highest energy image using the Dimer Method.

45
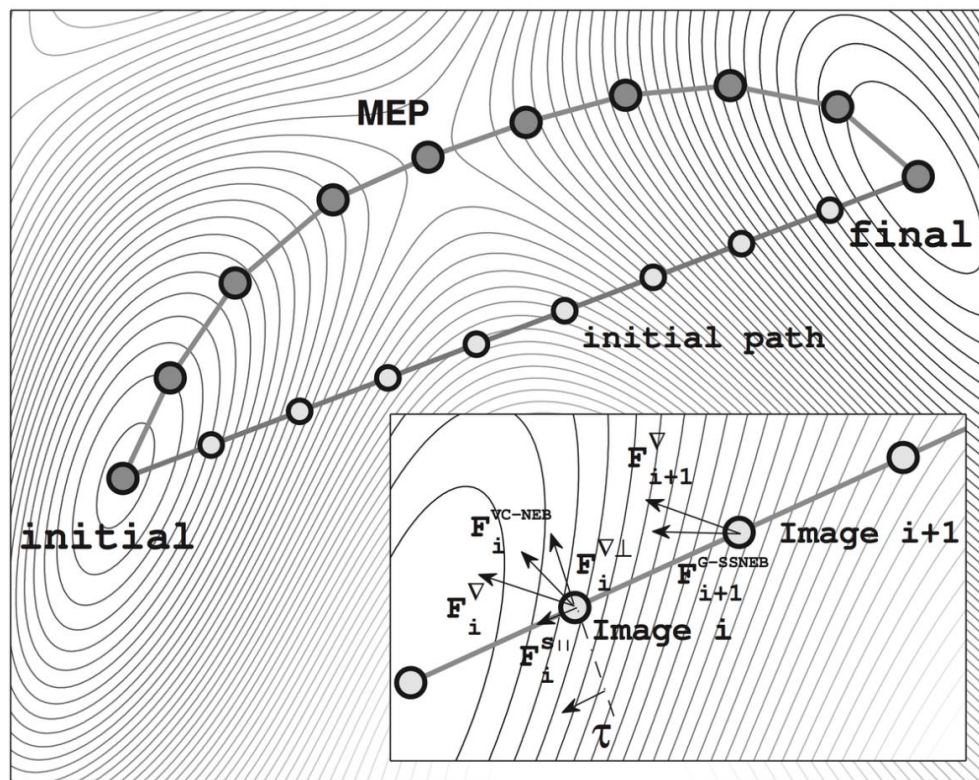
Figure 21: Example NEB Simulation showing initial images created (line with white circles) along a direct reaction path from initial to final. The final optimized path (line with gray circles) passes through the MEP of that specific reaction. This figure was taken from Jonsson et al.[75]

4.1.2 Dimer Method

The dimer method (or more generally a min-mode method) is used to find saddle points on a potential energy surface. It is complimentary to the nudged elastic band method because it does not require a final state.[74] This method can also be used to start from a minimum basin and search in random directions for saddle points. In some simple systems, reaction endpoints can be guessed, and the nudged elastic band can be used to find reaction pathways. Instead of creating more images effectively doubling the calculation time, the dimer method can be used instead to find the saddle point relatively easily. For a simple barrier like that of the simple mechanism used here it works well.[74]

46

4.2 Computational Methods

For the most part the details of the calculations are the same as those done in Chapter 2 and 3. Calculations based on density functional theory (DFT) were carried out using the VASP (Vienna ab initio simulation) package.[43] The PBE generalized gradient approximation (GGA) exchange-correlation potential[44] was used, and the electron-core interactions were treated in the projector augmented wave method[45, 46]. The van der Waals interaction was considered through DFT-D3 semi-empirical methods via a pairwise force field.[47, 48] Structures were optimized until the atomic forces were smaller than 0.02 eV Å−1 with a kinetic cutoff energy of 400 eV. Reaction barriers were determined with the Nudged Elastic Band method and the saddle point was found using the dimer method. NEB used 8 images and set the spring constant to 5.0 eV/Å^2 with nudging and it was set to the climbing image algorithm. The dimer separation was set to 0.01Å with a maximum of 6 rotation steps per translation and the rotational force range is 0.01-1.0.

All the calculations were performed using a ZSM-5 unit cell including 96 Si and 192 O atoms. The structure of the unit cell was taken from an experimental work (a = 20.078 Å; b = 19.894 Å; c = 13.372 Å)[53] and fixed during the calculation. Where this differs from chapter 2 and 3 is that in addition to the unit cell and water, hexane was added as the absorbed species on the acid sites instead of water. This was done with both a single BAS as well as two in the D2 configuration. To probe the impact of water, this was done without water, with 1 water molecule both in-between the BAS and the hexane and on the outside, and then the same with 3 water molecules. In addition, solvation effects were examined by finding how the barrier changed using implicit solvation as described in Chapter 3.

4.3 Results and Discussion

4.3.1 Hexane Protolytic Cracking for 1 BAS

As discussed in the introduction, the entirety of these results will be chemical potential barriers in order to determine sources of enhancement of the kinetics of protolytic cracking of n-hexane on HZSM-5. As was also mentioned, the mechanism that will be used will be that shown in Boronat et al.[18]. Starting off it is important to have a control barrier to compare to. In this case the control is a single acid site with a single hexane molecule and no water. This control barrier is shown in Figure 23.
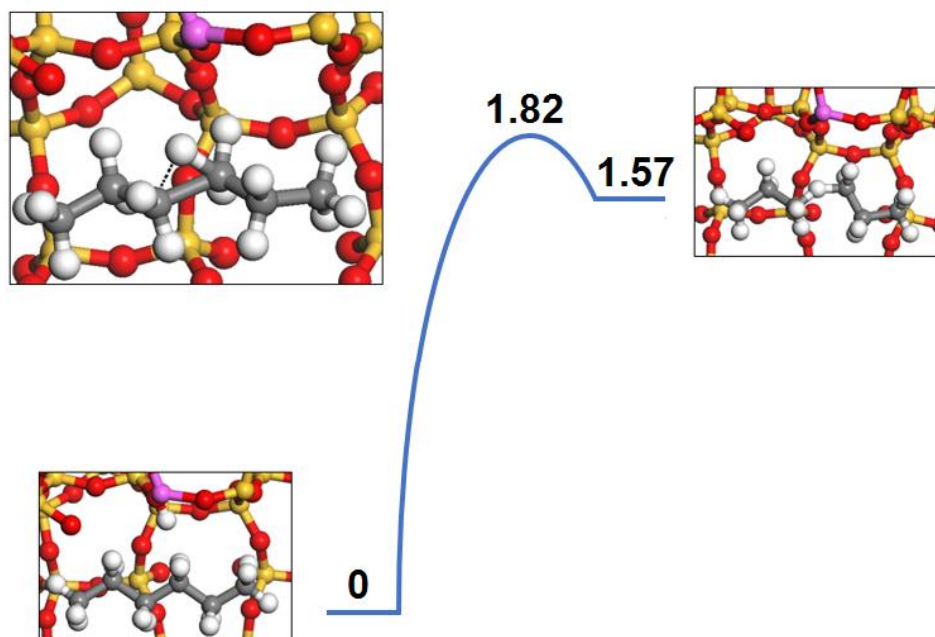
Figure 22: Protolytic Hexane Cracking Reaction Pathway. Energy listed in eV.

This barrier is significantly smaller than the one found by Boronat et al.[18] of 67 kcal/mol but significantly larger than the one found experimentally by Luknayov et al.[76] of 75.6–152.4 kJ/mol, the exact value in the range depending on the reaction products. 1.82eV is about equal to 42kcal/mol which is equal to 175.9 kJ/mol. As for the result

from Boronat et al., this was the same mechanism but that report used butane rather than hexane, which should have a slightly lower barrier for cracking since it is a larger alkane.[33] And for Luknayov et al., it is possible that the kinetics that were measured included some of the enhancements that will be discussed in this section. Either way, it is not the goal of this DFT study to provide rigorous kinetic parameters, but rather to simply investigate sources of enhancement to hexane cracking. So long as the barrier is of a similar scale to previously published work, it will work as a base of comparison.

With a control barrier of 1.82eV, the effect of water on the reaction can be examined. Keeping just 1 BAS for now, water was placed absorbed on the acid site and the hexane was then protonated by the hydronium as can be seen in Figure 24A. The order was switched for 24B where the hexane is protonated by the BAS as normal but the water serves to stabilize the charge by forming hydrogen bonds with zeolite wall. A hydrogen bond with the hexane does not form but the negative oxygen end comes close.
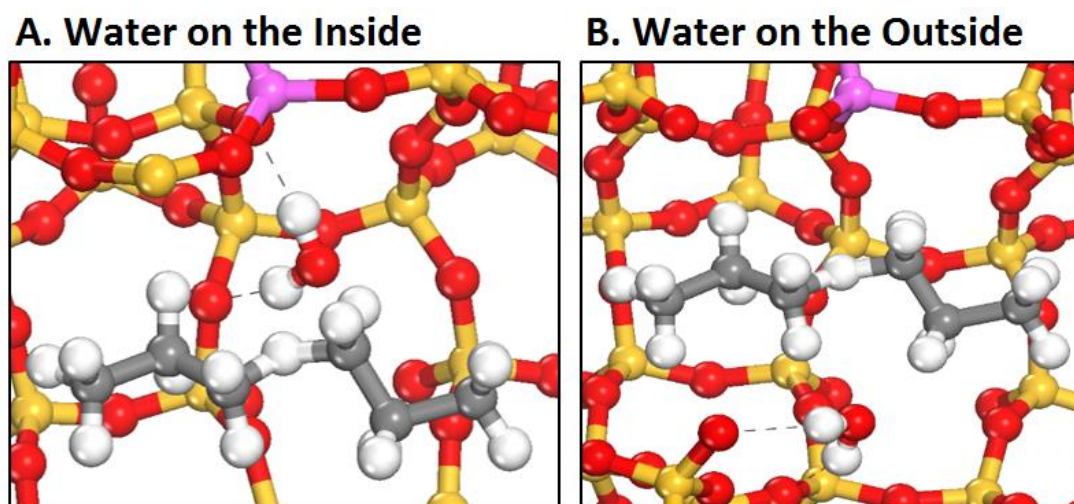
Figure 23: Position of the water during the reaction. Note for water on the inside it is one of the protons of the water that is transferred and the site is then deprotonated by the hydroxide. The dashed lines are hydrogen bonds.

The barriers for these different 1 water reactions are shown below in Figure 25. The water enhancement predicted in Chapter 2 turned out to be untrue as it raised the barrier nearly 0.2eV. It seemed that pushing the hexane further away from the wall caused a large amount of Van der Waals interactions to weaken and for the intermediate to be less stable as a result. For water on the outside, however, there was shown to be a small lowering of the barrier. This is assumed to be due to the hydrogen bonds that can be seen distributing the charge of the intermediate into the opposite zeolite wall. This enhancement is small enough that it is not quite convincing yet that it could overpower the detrimental effects of water demonstrated. For that we need to look at adding more water to the system.
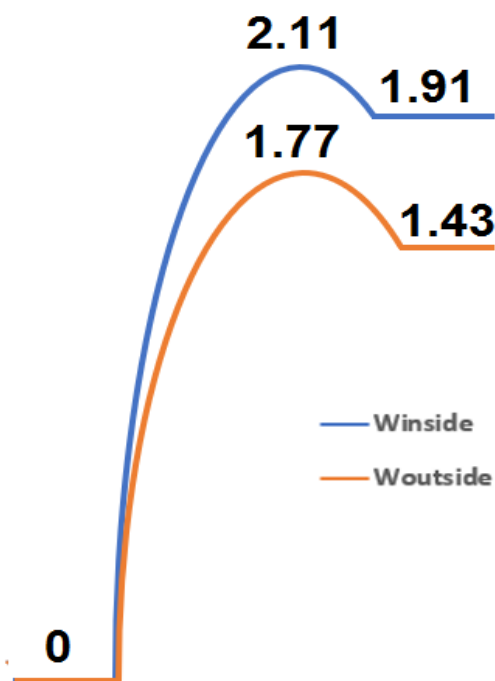
Figure 24: Kinetic barrier comparison between water being on the inside and outside. Energy listed in eV.

3 water molecules was chosen as the amount that could potentially be present in the small amounts used in Dr. Gumidyala's results.[14] In addition it fits naturally for there to be one water molecule for every bend in the hexane. The final structures of these barriers can be seen below in Figure 26. 26A is the same as 24B but it was relisted in order to more easily compare to the 3 water case. As can be seen in 26B, three water molecules function in much the same way as one, but they seem to have a tendency to chain in order to form as many hydrogen bonds with the zeolite wall as possible. In this way the charge is distributed and the intermediate stabilized much more than one water molecule could ever do.
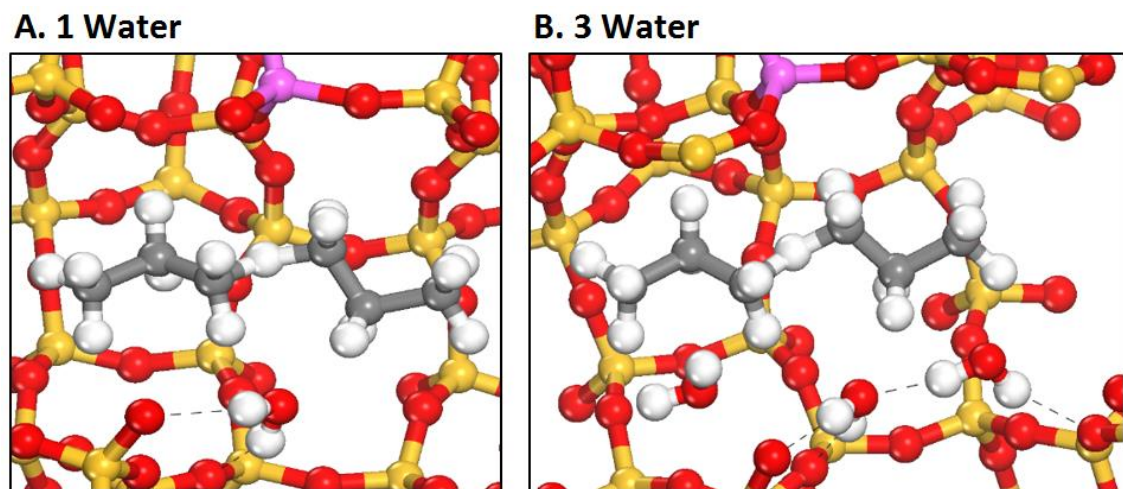
Figure 25: Number of water used for different reactions. The extra water serves to further stabilize the intermediate. The dashed lines are hydrogen bonds.

The barriers comparing the 1W and 3W case can be seen below in Figure 27. The result for 3 water molecule is another small enhancement, this time of 0.09eV compared to the case for 1W and resulting in a total of 0.14eV enhancement to the control. While 1W may have been an enhancement within the range of error, 0.14eV is much more significant appreciable as a realistic source of improved kinetics. This does not prove that this is enough to overpower the increased likelihood of water competitively absorbing or stripping sites but the possibility is increasing the lower the barrier gets. Now with some promising enhancement due to water, the next step is to look at where the enhancement from nearby BAS might be coming from.
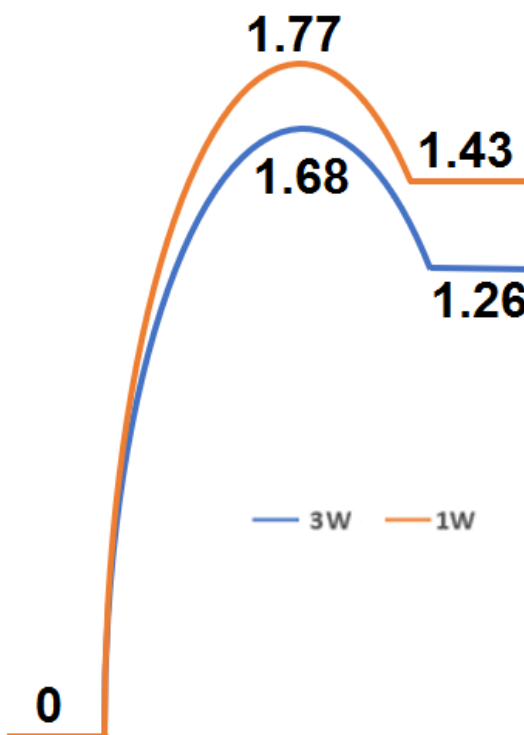
Figure 26: Kinetic barrier comparison between 1 water molecule and 3 water molecules. The 1 water case is for water on the outside. Energy listed in eV.

4.3.2 Combining Multiple BAS and Water Cluster Effects on Cracking

With the original theory of nearby BAS enhancing the reaction by turning the water into a hydronium disproven by the first set of barrier calculations, there had to be some other source of enhancement that multiple BAS offer. The theory that was tested is that of Kubarev et al.[11] where one BAS polarizes the alkane while the other is the proton donor. An example of what this looks like can be seen below in Figure 28. The BAS on the right side of the image is not participating, but the proposal is that the charge center will polarize the molecule so that the end by the acid site is more negative. This should then make it easier for the first BAS to split a carbon-carbon bond and protonate. This is shown to be true based on the barriers presented in the next page on Figure 29.
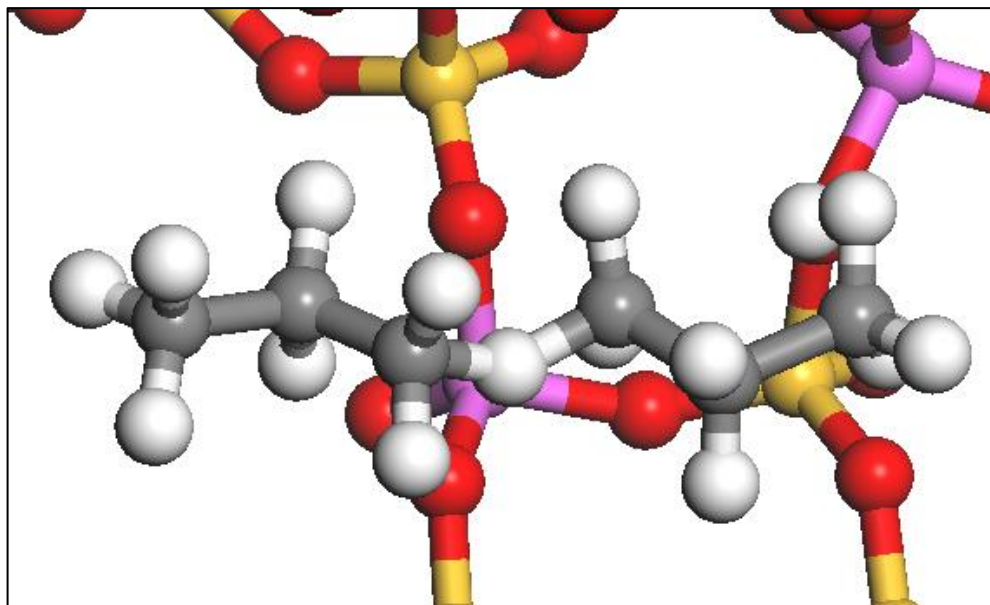
Figure 27: Optimized final state for 2BAS, no water. The enhancement is attributed to the nonparticipating BAS polarizing the hexane.
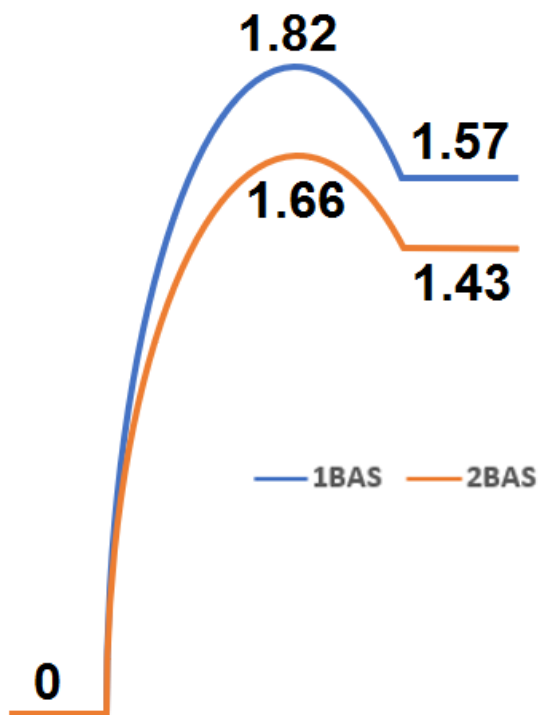
Figure 28: Kinetic barrier comparison of the effect of multiple acid site polarizing the hexane. Energy listed in eV.

This new setup is compared back to the control, and from this it can be seen how significant the enhancement due to this polarization is. It results in a lowering of the barrier by 0.16eV, even more than that of three water molecules. If both of these beneficial effects were to combine, that could begin to explain why Dr. Gumidyala saw enhanced conversion of cracking. With this in mind the next and final barriers were combining the effects of adjacent BAS polarization and water cluster stabilization. The final states for the barriers are shown on the next page in Figure 30. Here the water and adjacent BAS appear to function exactly the same as for previously cases when they were separate, Figure 26 and 28, respectively. The barriers are shown below it on Figure 31.
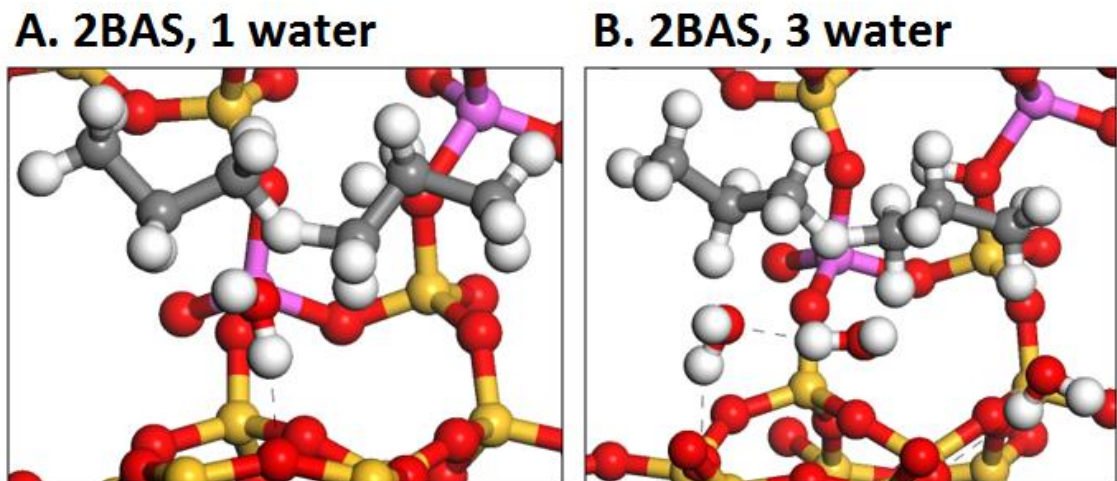
Figure 29: Structures for the combined water cluster and nearby BAS enhancements. The dashed lines are hydrogen bonds.
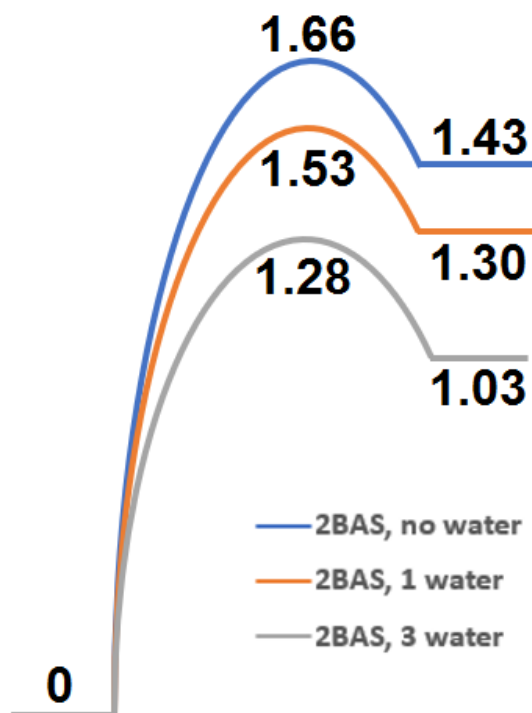
Figure 30: Kinetic barrier comparing all 2BAS cases. Energy listed in eV.

Looking at Figure 31, all combined the water cluster enhancements resulted in the barrier lowering by a staggering 0.38eV as compared to the case for 2BAS and no water. Combining that with the benefit from the BAS polarization and the total reaches 0.54eV, a huge amount in reference to the impact on kinetics. Given the right circumstances, a barrier lowering by that much could certainly double the rate or massively improve conversion, if not more than that. The requirements surrounding this enhancement are very specific and not likely to be beneficial in many reactions due to the negative impact of water, but it seems that if the enhancement occurs it could absolutely result in the results of Chen et al. and Dr. Gumidyala.[13, 14]

All of the calculated barriers are combined and compiled below in Table 5 for ease of comparison. There is not much to add on top of what has already been said but it is interesting to note that the benefit from the two sources is more than just additive. If that were the case the end benefit would have been around 0.3eV but instead it is 0.54. And in theory these benefits wouldn't necessarily be limited to hexane. The combination of high acid density and tight confinement are mostly unique to zeolites, but these same enhancements should be possible with other hydrocarbons and zeolites.

Table 5: All protolytic hexane cracking activation energy and heat of reaction tabulated. Arranged in the order presented in the text.

Configuration	E_A (eV)	ΔH (eV)
1BAS, no water	1.82	1.57
1BAS, 1W inside	2.11	1.91
1BAS, 1W outside	1.77	1.43
1BAS, 3W	1.68	1.26
2BAS, no water	1.66	1.43
2BAS, 1W	1.53	1.30
2BAS, 3W	1.28	1.03

4.3.3 Possible Drawbacks and Concerns

A couple of things must be said about these results before it is assumed that the benefits can be freely applied to all manner of zeolite catalyzed reactions. Firstly, this was mentioned multiple times throughout this section, but water is a deterrent to basically all petrochemical reactions. It is either a product of the reactions so it limits the reaction from Le Chatelier's principle or it competitively absorbs on sites and clogs up pores. In basically in every way other than the specific case show here water will only inhibit reaction kinetics. To better confirm whether this enhancement would overpower detrimental effects, a more in depth kinetic analysis of both water diffusion/absorption, and some experimental results would be necessary.

Secondly, the conditions surrounding the improvement due to polarization by nearby acid sites are very specific, too specific to be simply universally applicable to every low Si/Al ratio zeolite. The acid sites must be close enough that the hexane can comfortably reach and be affected by both acid sites, and ideally, they would be placed lengthwise along a pore or in the intersection so that the hexane would interact with them in its natural lengthwise orientation of diffusion down a pore. Such a combination of attributes likely would only occur under specific zeolite synthesis conditions. Since at least some degree of enhancement has been found experimentally by multiple sources[11, 13, 14], there should be some specific combination or combinations of solvent, precursor, and synthesis conditions that result in an ideal zeolite for this purpose. There is literature out there that could provide direction on this front but this is out of the scope of this project.

And finally, this is all just a theory at this point. The barrier results make it a promising theory, but there is only light experimental backing for many of the decisions made. The most glaring of these is the choice of mechanism for the hexane cracking. Hexane cracking as an enhanced reaction is supported by Dr. Gumidyala's results, but the exact mechanism is yet to be determined for sure. A very specific type of protolytic cracking was chosen for its simplicity and comparative ease in creating barriers from NEB calculations, but this was chosen more for reasons of being able to confirm enhancement theories than to discover the true mechanism that of that specific experiment. The reasons behind these enhancements as presented in this report should be looked at as an exciting possibility rather than proven at this stage of research. Hopefully in the future this possibility can be cemented into something beneficial to zeolite catalysis.

4.4 Conclusions

     The catalytically beneficial effects of water cluster interaction and acid site polarization of n-hexane cracking in HZSM-5 was studied using DFT NEB kinetic barrier calculations. A control barrier of 1.82eV was found for the protonation of hexane. Water, despite being generally considered detrimental to zeolite catalysis, showed some potential for reaction enhancement under specific conditions. When positioned on the outside of hexane during a standard protonation step in protolytic cracking, water appeared to stabilize the charged intermediate by forming hydrogen bonds with the reverse zeolite wall. This enhancement effect was compounded when 3 water molecules were placed instead of one. The result was a lowering of the barrier by 0.14eV.

     Nearby BAS also showed enhancement when in a certain configuration. Placed lengthwise along the straight channel, one acid site was shown to polarize the hexane before the other participated in the protonation. This cooperative effect had a very large impact on the barrier, lowering it by 0.16eV. With the two beneficial effects in combination the benefits compounded, with a greater result than the sum of their parts. The total benefit relative to the control barrier for 3 water and 2BAS configured as described was 0.54eV. Many of the details behind this general theory need some additional work but the results are very promising. For example, Gibbs free energies should be included in addition to the DFT-calculated total energies since the cracking reactions are normally conducted at moderate temperatures.

Chapter 5: Concluding Remarks and Future Work

In chapter 2, the effects of location and density of BAS on water adsorption in HZSM-5 was studied using DFT calculations. Adsorption energy of water grew significantly as the separation between BAS decreases because the water is polarized by both sites leading to the enhanced adsorption, which is evidenced by the directional charge transfer. These results suggest that in HZSM-5 and other high acid density zeolites, nearby acid sites, which exist in low Si/Al samples, may play a role in determining the molecular adsorption and reaction. In addition, from these results it is expected the proton delocalization from the zeolite framework into water may be more pronounced when a large water cluster or an aqueous phase is present in the system.

In chapter 3, the effects of water cluster interaction with BAS and preferential solvent diffusion in HZSM-5 was studied using DFT AIMD simulations. Water clusters were shown to be highly preferential locations for protons to be rather than the BAS of zeolites. This demonstrated the strong stripping ability of water and the power of stabilizing charged species in water clusters. In addition, water was shown to strongly selectively diffuse into the sinusoidal channel over the straight channel. This occurred for every AIMD simulation but was particularly evident for cases in which the pore was only partially filled such as with the 6 and 23 water molecule AIMD simulations. It is theorized that for water at least, the shape of the sinusoidal channel is better suited for the positioning of hydrogen bonds. The additional bonds lower the energy and makes the sinusoidal channel energetically the better place for water molecules to be located.

In chapter 4, the catalytically beneficial effects of water cluster interaction and acid site polarization of n-hexane cracking in HZSM-5 was studied using DFT NEB

kinetic barrier calculations. A control barrier of 1.82eV was found for the protonation of hexane. Water showed some potential for reaction enhancement under specific conditions, appearing to stabilize the charged intermediate by forming hydrogen bonds with the reverse zeolite wall. This enhancement effect was compounded when 3 water molecules were placed instead of one. The result was a lowering of the barrier by 0.14eV in total. Nearby BAS also showed enhancement when in a certain configuration. Placed lengthwise along the straight channel, one acid site was shown to polarize the hexane before the other participated in the protonation. This cooperative effect had a very large impact on the barrier, lowering it by 0.16eV. The two beneficial effects in combination compounded, for a grand total of a 0.54eV decrease in the control barrier.

As discussed at the end of chapter 4, these proposed enhancements are just a theory. Being proven will require much more evidence, especially experimental evidence. In addition, there is an argument to be had for the enhancement to not necessarily be two BAS. Research into cooperative interaction between Brønsted and Lewis acid sites could be important to fully understand the possible causes for enhancement. Another natural places for future work to spring off this project would be to try another cracking reaction, such as cumene cracking. This reaction occurs at lower temperature and thus would be less impaired by water stripping like hexane cracking is. There are similar enhancements for this reaction so this could be a good project to start a new student. Hopefully some future researchers at OU or elsewhere can pick up where this project left off and better understand the sources of the bizarre zeolite reaction enhancement. There is certainly potential here and it would be a waste for it to go untapped. To any who come next, I wish them luck and hope my thesis can be of some help.

References

1.   Payra, P.a.D., Prabir K., *Zeolites: A Primer.* Marcel Dekker Inc., 2003: p. 19.

2.   Splettstoesser, T., *The microporous molecular structure of a zeolite, ZSM-5*, Zeolite-ZSM-5-vdW.png, Editor. 2015.

3.   Corma, A., *From Microporous to Mesoporous Molecular Sieve Materials and Their Use in Catalysis.* Chem. Rev., 1997. **97**: p. 2373-2419.

4.   Hattori, H., and Yoshiow Ono, *Solid Acid Catalysis: from Fundamentals to Applications*. 2015: Pan Stanford Publishing.

5.   Ghorbanpour, A., J.D. Rimer, and L.C. Grabow, *Periodic, vdW-corrected density functional theory investigation of the effect of Al siting in H-ZSM-5 on chemisorption properties and site-specific acidity.* Catalysis Communications, 2014. **52**: p. 98-102.

6.   Bhan, A. and E. Iglesia, *A link between reactivity and local structure in acid catalysis on zeolites.* Accounts of Chemical Research, 2008. **41**(4): p. 559-567.

7.   Shirazi, L., E. Jamshidi, and M.R. Ghasemi, *The effect of Si/Al ratio of ZSM-5 zeolite on its morphology, acidity and crystal size.* Crystal Research and Technology, 2008. **43**(12): p. 1300-1306.

8.   Janda, A. and A.T. Bell, *Effects of Si/Al ratio on the distribution of framework Al and on the rates of alkane monomolecular cracking and dehydrogenation in H-MFI.* J Am Chem Soc, 2013. **135**(51): p. 19193-207.

9.   Vjunov, A., et al., *Quantitatively probing the Al distribution in zeolites.* J Am Chem Soc, 2014. **136**(23): p. 8296-306.

10.   Mlinar, A.N., et al., *Effects of Bronsted-acid site proximity on the oligomerization of propene in H-MFI.* Journal of Catalysis, 2012. **288**: p. 65-73.

11.   Kubarev, A.V., et al., *Solvent Polarity-Induced Pore Selectivity in H-ZSM-5 Catalysis.* ACS Catal, 2017. **7**(7): p. 4248-4252.

12.   Capelle, K., *A Bird's-Eye View of Density-Functional Theory.* Cornell University Library, 2006. **arXiv:cond-mat/0211443**: p. 69.

13.   Chen, K., et al., *Trace water amounts can increase benzene H/D exchange rates in an acidic zeolite.* Journal of Catalysis, 2017. **351**: p. 130-135.

14.   Gumidyala, A., *Vapor Phase Upgrading of Renewable Carboxylic Acids and Oxygenates over Bronsted Zeolites*, in *Department of Chemical, Biological, & Materials Engineering*. 2017, University of Oklahoma.

15.   Ohlin, L., et al., *Adsorption of CO2, CH4, and H2O in Zeolite ZSM-5 Studied Using In Situ ATR-FTIR Spectroscopy.* The Journal of Physical Chemistry C, 2013. **117**(33): p. 16972-16982.

16.   Song, C.H., et al., *Cooperativity of adjacent Bronsted acid sites in MFI zeolite channel leads to enhanced polarization and cracking of alkanes.* Journal of Catalysis, 2017. **349**: p. 163-174.

17.   Vjunov, A., et al., *Tracking the Chemical Transformations at the Brønsted Acid Site upon Water-Induced Deprotonation in a Zeolite Pore.* Chemistry of Materials, 2017.

18.   Boronat, M. and A. Corma, *Are carbenium and carbonium ions reaction intermediates in zeolite-catalyzed reactions?* Applied Catalysis A: General, 2008. **336**(1-2): p. 2-10.

19.   Dedecek, J., Z. Sobalik, and B. Wichterlova, *Siting and Distribution of Framework Aluminium Atoms in Silicon-Rich Zeolites and Impact on Catalysis.* Catalysis Reviews-Science and Engineering, 2012. **54**(2): p. 135-223.

20.   Di Iorio, J.R. and R. Gounder, *Controlling the Isolation and Pairing of Aluminum in Chabazite Zeolites Using Mixtures of Organic and Inorganic Structure-Directing Agents.* Chemistry of Materials, 2016. **28**(7): p. 2236-2247.

21.   Gabova, V., J. Dedecek, and J. Cejka, *Control of Al distribution in ZSM-5 by conditions of zeolite synthesis.* Chemical Communications, 2003(10): p. 1196-1197.

22.   Dedecek, J., et al., *Synthesis of ZSM-5 Zeolites with Defined Distribution of Al Atoms in the Framework and Multinuclear MAS NMR Analysis of the Control of Al Distribution.* Chemistry of Materials, 2012. **24**(16): p. 3231-3239.

23.   Pashkova, V., et al., *Incorporation of Al at ZSM-5 hydrothermal synthesis. Tuning of Al pairs in the framework.* Microporous and Mesoporous Materials, 2015. **202**: p. 138-146.

24.   Perea, D.E., et al., *Determining the location and nearest neighbours of aluminium in zeolites with atom probe tomography.* Nature Communications, 2015. **6**.

25.   Yu, Z., et al., *Brønsted/Lewis Acid Synergy in H–ZSM-5 and H–MOR Zeolites Studied by1H and27Al DQ-MAS Solid-State NMR Spectroscopy.* The Journal of Physical Chemistry C, 2011. **115**(45): p. 22320-22327.

26.   Xu, B., et al., *Effect of framework Si/Al ratio and extra-framework aluminum on the catalytic activity of Y zeolite.* Applied Catalysis A: General, 2007. **333**(2): p. 245-253.

27. Simon-Masseron, A., et al., *Influence of the Si/Al ratio and crystal size on the acidity and activity of HBEA zeolites.* Applied Catalysis A: General, 2007. **316**(1): p. 75-82.

28. Jones, A.J., et al., *Acid strength and solvation in catalysis by MFI zeolites and effects of the identity, concentration and location of framework heteroatoms.* Journal of Catalysis, 2014. **312**: p. 58-68.

29. Yeh, Y.-H., et al., *Adsorption of Small Alkanes on ZSM-5 Zeolites: Influence of Brønsted Sites.* The Journal of Physical Chemistry C, 2016. **120**(22): p. 12132-12138.

30. Xu, B., et al., *Effect of framework Si/Al ratio and extra-framework aluminum on the catalytic activity of Y zeolite.* Applied Catalysis a-General, 2007. **333**(2): p. 245-253.

31. Kramer, G.J. and R.A. Vansanten, *Theoretical Determination of Proton Affinity Differences in Zeolites.* Journal of the American Chemical Society, 1993. **115**(7): p. 2887-2897.

32. Sierka, M., et al., *Heterogeneity of Bronsted acidic sites in faujasite type zeolites due to aluminum content and framework structure.* Journal of Physical Chemistry B, 1998. **102**(33): p. 6397-6404.

33. Gounder, R. and E. Iglesia, *Catalytic Consequences of Spatial Constraints and Acid Site Location for Monomolecular Alkane Activation on Zeolites.* Journal of the American Chemical Society, 2009. **131**(5): p. 1958-1971.

34. Wang, M., et al., *Remarkable acceleration of the fructose dehydration over the adjacent Bronsted acid sites contained in an MFI-type zeolite channel.* Journal of Catalysis, 2014. **319**: p. 150-154.

35. Sazama, P., et al., *Effect of aluminium distribution in the framework of ZSM-5 on hydrocarbon transformation. Cracking of 1-butene.* Journal of Catalysis, 2008. **254**(2): p. 180-189.

36. Janda, A. and A.T. Bell, *Effects of Si/Al Ratio on the Distribution of Framework Al and on the Rates of Alkane Monomolecular Cracking and Dehydrogenation in H-MFI.* Journal of the American Chemical Society, 2013. **135**(51): p. 19193-19207.

37. Sharada, S.M., et al., *Insights into the Kinetics of Cracking and Dehydrogenation Reactions of Light Alkanes in H-MFI.* Journal of Physical Chemistry C, 2013. **117**(24): p. 12600-12611.

38. Janda, A., et al., *Effects of Zeolite Structural Confinement on Adsorption Thermodynamics and Reaction Kinetics for Monomolecular Cracking and Dehydrogenation of n-Butane.* J Am Chem Soc, 2016. **138**(14): p. 4739-56.

39.   Sohn, J.R., et al., *Acid Catalysis by Dealuminated Zeolite-Y .2. The Roles of Aluminum.* Journal of Physical Chemistry, 1986. **90**(20): p. 4847-4851.

40.   Haag, W.O., R.M. Lago, and P.B. Weisz, *The Active-Site of Acidic Aluminosilicate Catalysts.* Nature, 1984. **309**(5969): p. 589-591.

41.   Gounder, R. and E. Iglesia, *The catalytic diversity of zeolites: confinement and solvation effects within voids of molecular dimensions.* Chemical Communications, 2013. **49**(34): p. 3491-3509.

42.   Ernzerhof, J.H.G.E.S.M., *Hybrid functionals based on a screened Coulomb potential.* J. Chem. Phys., 2003. **118**(18).

43.   G. Kresse, J.F., *Efficient iterative schemes for ab initio total-energy calculations using a plane-wave basis set.* Phys. Rev. B Condens, 1996. **54**: p. 11169–11186.

44.   J. P. Perdew, K.B., M. Ernzerhof, *Generalized gradient approximation made simple.* Phys. Rev. Lett., 1996. **77**: p. 3865–3868.

45.   Blöchl, P.E., *Projector augmented-wave method.* Physical Review B, 1994. **50**(24): p. 17953-17979.

46.   G. Kresse, D.J., *From ultrasoft pseudopotentials to the projector augmented-wave method.* Phys. Rev. B, 1999. **59**: p. 1758–1775.

47.   Grimme, S., et al., *A consistent and accurate ab initio parametrization of density functional dispersion correction (DFT-D) for the 94 elements H-Pu.* J Chem Phys, 2010. **132**(15): p. 154104.

48.   Grimme, S., S. Ehrlich, and L. Goerigk, *Effect of the damping function in dispersion corrected density functional theory.* J Comput Chem, 2011. **32**(7): p. 1456-65.

49.   Heyd, J., G.E. Scuseria, and M. Ernzerhof, *Hybrid functionals based on a screened Coulomb potential.* The Journal of Chemical Physics, 2003. **118**(18): p. 8207-8215.

50.   A. J. Cohen, P.M.-S., W. Yang, *Insights into current limitations of density functional theory.* Science 2008. **321**: p. 792–794.

51.   Gumidyala, A., B. Wang, and S. Crossley, *Direct carbon-carbon coupling of furanics with acetic acid over Bronsted zeolites.* Science Advances, 2016. **2**(9).

52.   Duong, N.N., et al., *Enhancing the Acylation Activity of Acetic Acid by Formation of an Intermediate Aromatic Ester.* Chemsuschem, 2017. **10**(13): p. 2823-2832.

53.   Koningsveld, H.v., *High-temperature (350 K) orthorhombic framework structure of zeolite H-Zsm-5.* Acta Crystallogr. B, 1990. **46**: p. 731–735.

54.   Jones, A.J. and E. Iglesia, *The Strength of Bronsted Acid Sites in Microporous Aluminosilicates.* Acs Catalysis, 2015. **5**(10): p. 5741-5755.

55.   Iglesia, R.G.a.E., *Catalytic Consequences of Spatial Constraints and Acid Site Location for Monomolecular Alkane Activation on Zeolites.* J. AM. CHEM. SOC., 2009. **131**: p. 1958–1971.

56.   Shi, H., et al., *Tailoring nanoscopic confines to maximize catalytic activity of hydronium ions.* Nat Commun, 2017. **8**: p. 15442.

57.   Sklenak, S., et al., *Aluminum siting in silicon-rich zeolite frameworks: A combined high-resolution Al-27 NMR spectroscopy and quantum mechanics/molecular mechanics study of ZSM-5.* Angewandte Chemie-International Edition, 2007. **46**(38): p. 7286-7289.

58.   Kim, H., et al., *On methanol to hydrocarbons reactions in a hierarchically structured ZSM-5 zeolite catalyst.* Catalysis Today, 2017.

59.   Olson, D.H.K., N.; Peters, A. W.; Toby, B. H., *Crystal Structure of Dehydrated CsZSM-5 (5.8Al): Evidence for Nonrandom Aluminum Distribution.* J. Phys. Chem. B., 2000(104): p. 4844.

60.   Mentzen, B.F.B., G.; Emerich, H.; Weber, H.-P., *Dehydrated and Cs+ Exchanged MFI Zeolites: Location and Population of Cs+ from In Situ Diffraction Data as a Function of Temperature and Degree of Exchange.* J. Phys. Chem. B, 2006(110): p. 97.

61.   Kim, C.W., N.H. Heo, and K. Seff, *Framework Sites Preferred by Aluminum in Zeolite ZSM-5. Structure of a Fully Dehydrated, Fully Cs+-Exchanged ZSM-5 Crystal (MFI, Si/Al = 24).* The Journal of Physical Chemistry C, 2011. **115**(50): p. 24823-24838.

62.   Biligetu, T., et al., *Al distribution and catalytic performance of ZSM-5 zeolites synthesized with various alcohols.* Journal of Catalysis, 2017. **353**: p. 1-10.

63.   Derouane, E.G., et al., *The Acidity of Zeolites: Concepts, Measurements and Relation to Catalysis: A Review on Experimental and Theoretical Methods for the Study of Zeolite Acidity.* Catalysis Reviews, 2013. **55**(4): p. 454-515.

64.   Resasco, D.E., B. Wang, and S. Crossley, *Zeolite-catalysed C-C bond forming reactions for biomass conversion to fuels and chemicals.* Catalysis Science & Technology, 2016. **6**(8): p. 2543-2559.

65.   Zapata, P.A., et al., *Hydrophobic Zeolites for Biofuel Upgrading Reactions at the Liquid-Liquid Interface in Water/Oil Emulsions.* Journal of the American Chemical Society, 2012. **134**(20): p. 8570-8578.

66.   D.H. Olson, W.O.H., W.S. Borghard, *Use of water as a probe of zeolitic properties: interaction of water with HZSM-5.* Microporous and Mesoporous Materials, 2000. **35–36**: p. 435–446.

67.   A. G. Pelmenschikov, E.A.P., M. 0. Edisherashvili, and G. M. Zhidomirov, *On the Loewenstein Rule and Mechanism of Zeolite Deaiumination.* J. Phys. Chem., 1992. **96**(No. 17,).

68.   Henkelman, G., A. Arnaldsson, and H. Jonsson, *A fast and robust algorithm for Bader decomposition of charge density.* Computational Materials Science, 2006. **36**(3): p. 354-360.

69.   Burt, T.A., *IMPROVING THE THERMAL CONDUCTIVITY OF NANOTUBE COMPOSITES VIA END FUNCTIONALIZATON: RANDOM WALKS AND MOLECULAR DYNAMICS*, in *Department of Engineering Physics*. 2017, University of Oklahoma: Norman, OK.

70.   Skyner, R.E., et al., *A review of methods for the calculation of solution free energies and the modelling of systems in solution.* Phys Chem Chem Phys, 2015. **17**(9): p. 6174-91.

71.   Humphrey, W., Dalke, A. and Schulten, K., *VMD - Visual Molecular Dynamics.* J. Molec. Graphics, 1996. **14**: p. 33-38.

72.   Vjunov, A., et al., *Impact of Zeolite Aging in Hot Liquid Water on Activity for Acid-Catalyzed Dehydration of Alcohols.* J Am Chem Soc, 2015. **137**(32): p. 10374-82.

73.   Zimmerman, P.M., et al., *Ab initio simulations reveal that reaction dynamics strongly affect product selectivity for the cracking of alkanes over H-MFI.* J Am Chem Soc, 2012. **134**(47): p. 19468-76.

74.   Hannes Jonsson, G.M., and Karsten W. Jacobsen, *Nudged elastic band method for finding minimum energy paths of transitions.* University of Texas, 2010.

75.   A.R. Oganov, C.W.G., A.O. Lyakhov, Q. Zhu, G.-R. Qian, H.T. Stokes, P. Bushlanov, Z. Allahyari, S. Lepeshkin, *USPEX 9.4.4 Manual: Variable-Cell Nudged-Elastic-Band (VCNEB) method.* Universal Structure Predictor: Evolutionary Xtallography, 2016.

76.   D.B Lukyanov, V.I.S., S.N. Khadzhiev, *A kinetic model for the hexane cracking reaction over H-ZSM-5.* Journal of Catalysis, 1994. **146**(1): p. 87-92.